PHD and CPHD Filtering with Unknown Detection Probability

Article *in* IEEE Transactions on Signal Processing · May 2018

DOI: 10.1109/TSP.2018.2835398

5 authors, including:

Wenguang Wang
Beihang University (BUAA)
40 PUBLICATIONS **279** CITATIONS

SEE PROFILE

Peng Lei
China University of Geosciences
19 PUBLICATIONS **208** CITATIONS

SEE PROFILE

PHD and CPHD Filtering With Unknown Detection Probability

Chenming Li, Wenguang Wang, Thia Kirubarajan, *Senior Member, IEEE*, Jinping Sun, and Peng Lei

***Abstract*— *A priori* knowledge of target detection probability is of critical importance in the Gaussian mixture probability hypothesis density (PHD) and cardinalized PHD (CPHD) filters. In addition, these two filters require that the process noise and measurement noise of the state propagated in the recursion be Gaussian. These limitations may restrict the two filters application in real problems. To accommodate unknown target detection probability and nonnegative non-Gaussian parameters, this paper proposes a new implementation based on inverse gamma Gaussian mixtures, introducing a location independent feature whose posterior probability density and likelihood function are nonnegative non-Gaussian inverse gamma and gamma functions to determine detection probability incorporated into the recursions. The derivation of the merging inverse gamma components is also presented to prevent the unbounded increase of mixture components by minimizing the Kullback–Leibler divergence. First, a real heavy-clutter scenario is used to validate the effectiveness of the proposed filters in track initiation and target tracking without known detection probability. Then, simulations are presented to demonstrate that the proposed CPHD and PHD filters can achieve multitarget tracking performance similar to the standard counterparts with known target detection probability, and that they outperform the standard counterparts in scenarios with unknown and dynamically changing detection probability. The robustness of the proposed filters is tested in both real and simulation scenarios. It is also shown that the analytical and empirical computational complexities of the proposed filters are similar to those of their standard counterparts.**

***Index Terms*—Probability hypothesis density (PHD) filter, Cardinalized PHD (CPHD) filters, inverse gamma Gaussian mixture, multitarget tracking, unknown target detection probability.**

I. Introduction

THE intent of multitarget tracking is to estimate the number of targets and their individual states using a set of measurements at one time or over a sliding-window. Recently, the probability hypothesis density (PHD) and cardinalized PHD (CPHD) filters developed using the random finite set (RFS) approach have attracted significant attention in multitarget tracking research [1]–[3]. Both of these Bayesian filters propagate the first-order multitarget moments known as target intensity through a two-step procedure: prediction and update. To mitigate the poor accuracy of the cardinality estimates in the PHD filter, the CPHD filter also propagates the cardinality distribution [2]. There are two implementations of the PHD and CPHD filters, one based on the Gaussian mixtures (GM) model [4], [5], and the other based on the sequential Monte Carlo (SMC) model [6].

The standard PHD and CPHD filters require some a priori models and parameters: the clutter model, the birth target model, and the target detection probability. These models are usually scenario-dependent, time-varying and are not known exactly in practical applications. Significant mismatches in the unknown model parameters will result in the degradation of tracking results. The first two unknown models (i.e., clutter and target birth) have been studied extensively in the literature. For the unknown clutter model, methods based on a clutter generator [9]–[12] are commonly used. These methods assume that the instances of clutter in the measurement space are generated by clutter generators [7], [8], and obtain clutter estimates by tracking the clutter generators. For the unknown target birth model, the main idea is to construct birth intensity from the measurements. A measurements-driven method called the diffuse target birth model was proposed in [13]–[15]. Another method to handle unknown target birth process is a partially uniform birth (PUB) model [16], [17]. In the unknown detection probability case, many methods have been proposed in recent years [18]–[20]. In [18], an adaptive tracker based on a Bayesian framework is proposed, but this tracker is applied to single target tracking; and in [19] a multi-target tracking method based on the belief propagation scheme is proposed. These two methods can tackle the situation where the detection probability is unknown and changes rapidly. However, they can't benefit from the RFS filter. In [20], a robust multi-Bernoulli filter is proposed; this filter uses Beta distribution to model the detection probability as [9], but this method requires a high detection probability. The three filters include the detection probability into the target state and then obtain the estimates. Despite this rich body of work, there is little research related to the unknown detection probability based on the GM CPHD/PHD model. To the best of our knowledge, the only work to date is in [9]. In [9], it is assumed that the current detection probability is determined by the historical detection probability, offering a Beta-Gaussian mixture

Manuscript received May 9, 2017; revised September 11, 2017, November 5, 2017, December 22, 2017, and April 9, 2018; accepted May 2, 2018. Date of publication May 10, 2018; date of current version June 12, 2018. The associate editor coordinating the review of this manuscript and approving it for publication was Dr. Paolo Braca. This work was supported by the National Natural Science Foundation of China under Grants 61771028 and 61471019. *(Corresponding author: Wenguang Wang.)*

C. Li, W. Wang, J. Sun, and P. Lei are with the School of Electronic and Information Engineering, Beihang University, Beijing 100191, China (e-mail: lchm1990@163.com; wwenguang@buaa.edu.cn; sunjinping@buaa.edu.cn; peng.lei@buaa.edu.cn).

T. Kirubarajan is with the Electrical and Computer Engineering Department, McMaster University, Hamilton, ON L8S 4K1, Canada (e-mail: kiruba@mcmaster.ca).

Color versions of one or more of the figures in this paper are available online at http://ieeexplore.ieee.org.

Digital Object Identifier 10.1109/TSP.2018.2835398

model for implementation. When the initialization of the historical detection probability is poor, the filters performance suffers. Furthermore, this filter requires that parameters be set manually. Poor selection of these parameters can adversely affect the models performance and robustness.

The target detection probability depends on the sensor, target, environment, and the features used for detection. The features most widely used in detection are the amplitude and the signal-to-noise ratio (SNR) [21]–[23]. Generally, stronger target amplitude and higher SNR will produce higher target detection probability, thus we can exploit target amplitude information to improve the PHD and CPHD filters with unknown detection probability. Due to the nonnegativity of the target amplitude and SNR, as well as the non-Gaussian noise, the target amplitude and SNR information cannot be incorporated directly into the standard PHD and CPHD filters with Gaussian models. In order to address this limitation, we exploit the inverse gamma Gaussian mixture (IGGM) distribution to implement the PHD and CPHD filters. We assume that the SNR feature is modeled using the inverse gamma component, with the additional assumption that the feature is position independent. It is possible to model other nonnegative features, e.g., target size [24], using this distribution as well.

The main contribution of this paper is the derivation of a closed-form solution to the CPHD recursion based on the inverse gamma Gaussian mixture model. Its intent is to exploit the inverse gamma component to propagate nonnegative features, including signal amplitude and SNR, that are non-Gaussian. This IGGM filter does not increase the complexity of the standard CPHD filter. Based on this solution, we also develop the following:

- An efficient filter to accommodate the unknown and changing target detection probability for multitarget tracking.
- Solutions to merge the inverse gamma components to prevent the unbounded increase of mixture components.
- An extended closed-form solution to the inverse gamma Gaussian mixture PHD filter.

The paper is organized as follows. Section II presents the background material on the standard CPHD/PHD filter, and the gamma and inverse gamma distributions. Section III shows how the inverse gamma Gaussian mixture can be used to implement the CPHD and PHD filters. The merging procedure of the inverse gamma components is also delineated in this section. The performance of the proposed method is demonstrated on real and simulated scenarios in Section IV: First, a real heavy-clutter scenario is used to validate the effectiveness of the proposed filters in track initiation and target tracking without known detection probability against the Interacting Multiple Model (IMM) technique combined with Multiple Hypothesis Tracking (MHT) algorithm and the Probabilistic Data Association (PDA) algorithm. Conclusions are presented in Sections V.

II. Background

A. The Standard CPHD and PHD Filter

Let $\mathbf{x}$ and $\mathbf{z}$ denote a single target state vector and a measurement vector, respectively. At time k, multitarget states and sensor measurements can be represented respectively as finite sets

$$X_k = \{\mathbf{x}_{k,1}, ..., \mathbf{x}_{k,n(k)}\}, Z_k = \{\mathbf{z}_{k,1}, ..., \mathbf{z}_{k,m(k)}\} \quad (1)$$

where $n(k)$ and $m(k)$ are the cardinalities of targets and measurements, respectively. The multitarget states set X_k is the union of the surviving target states and the newborn target states. The sensor measurement set Z_k is the union of the measurement generated from targets and clutter.

Let $f_{k-1}(X_{k-1}|Z_{1:k-1})$ be the multitarget posterior density at time $k-1$, where $Z_{1:k-1} = Z_1, ..., Z_{k-1}$ are the cumulative measurements up to time $k-1$. The multitarget density propagated through prediction and update steps in the Bayesian framework can now be written as [3]

$$f_{k|k-1}(X|Z_{1:k-1}) = \int f_{k|k-1}(X|X')f_{k-1}(X'|Z_{1:k-1})\delta X' \quad (2)$$

$$f_k(X|Z_{1:k}) = \frac{f_k(Z_k|X)f_{k|k-1}(X|Z_{1:k-1})}{\int f_k(Z_k|X)f_{k|k-1}(X|Z_{1:k-1})\delta X} \quad (3)$$

where $\int \cdot \delta X$ denotes the set integral, $f_{k|k-1}(X|X')$ is the multitarget transition density, and $f_k(Z_k|X)$ is the likelihood function. The standard CPHD filter with target intensity $v(\mathbf{x})$ and cardinality distribution $\rho(n)$ has been derived in [2].

The prediction step of the CPHD filter is given by

$$v_{k|k-1}(\mathbf{x}) = \gamma_k(\mathbf{x}) + \int p_{S,k}(\mathbf{x}')f_{k|k-1}(\mathbf{x}|\mathbf{x}')v_{k-1}(\mathbf{x}')d\mathbf{x}' \quad (4)$$

$$\rho_{k|k-1}(n) = \sum_{j=0}^{n} \rho_{\Gamma,k}(n-j)\Pi_{k|k-1}[v_{k-1}, \rho_{k-1}](j) \quad (5)$$

where at time k, $\gamma_k(\cdot)$ is the target birth intensity function, while $p_{S,k}(\mathbf{x}')$ and $f_{k|k-1}(\mathbf{x}|\mathbf{x}')$ denote the target survival probability and Markov transition density with state $\mathbf{x}'$, respectively. The cardinality distribution function is denoted by $\rho_{\Gamma,k}(\cdot)$, and $\Pi_{k|k-1}[v, \rho](j)$ is as follows:

$$\Pi_{k|k-1}[v, \rho](j) = \sum_{l=j}^{\infty} C_j^l \rho(l) \frac{\langle p_{S,k}, v\rangle^j \langle 1 - p_{S,k}, v\rangle^{l-j}}{\langle 1, v\rangle^l} \quad (6)$$

where $C_j^l = l!/j!(l-j)!$ is the binomial coefficient and $C_j^l = 0$ for $j > l$, $\langle \cdot, \cdot \rangle$ is the inner product, and $\langle \alpha, \beta \rangle = \int \alpha(\mathbf{x})\beta(\mathbf{x})d\mathbf{x}$ when α, β are real valued functions, or $\langle \alpha, \beta \rangle = \sum_{l=0}^{\infty} \alpha(l)\beta(l)$ when α, β are real sequences.

Also, the update step can be given as

$$v_k(\mathbf{x}) = v_{k|k-1}(\mathbf{x}) \left[q_{D,k}(\mathbf{x}) \frac{\langle \Upsilon_k^1[v_{k|k-1}, Z_k], \rho_{k|k-1}\rangle}{\langle \Upsilon_k^0[v_{k|k-1}, Z_k], \rho_{k|k-1}\rangle} + \sum_{\mathbf{z}\in Z_k} \psi_{k,\mathbf{z}}(\mathbf{x}) \frac{\langle \Upsilon_k^1[v_{k|k-1}, Z_k - \{\mathbf{z}\}], \rho_{k|k-1}\rangle}{\langle \Upsilon_k^0[v_{k|k-1}, Z_k], \rho_{k|k-1}\rangle} \right] \quad (7)$$

$$\rho_k(n) = \frac{\Upsilon_k^0[v_{k|k-1}, Z_k](n)\rho_{k|k-1}(n)}{\langle \Upsilon_k^0[v_{k|k-1}, Z_k], \rho_{k|k-1}\rangle} \quad (8)$$

where

$$\Upsilon_k^u[v,Z](n) = \sum_{j=0}^{\min(|Z|,n)} (|Z|-j)!\rho_{K,k}(|Z|-j) \cdot P_{j+u}^n \frac{\langle q_{D,k}, v\rangle^{n-(j+u)}}{\langle 1, v\rangle^n} e_j(\Xi_k(v,Z)) \quad (9)$$

$$\Xi_k(v,Z) = \{\langle v, \psi_{k,\mathbf{z}}\rangle : \mathbf{z} \in Z\} \quad (10)$$

$$\psi_{k,\mathbf{z}}(\mathbf{x}) = \frac{\langle 1, \kappa_k\rangle}{\kappa_k(\mathbf{z})} g_k(\mathbf{z}|\mathbf{x}) p_{D,k}(\mathbf{x}) \quad (11)$$

$$q_{D,k}(\mathbf{x}) = 1 - p_{D,k}(\mathbf{x}) \quad (12)$$

where at time k, $p_{D,k}(\mathbf{x})$ is the target detection probability, $g_k(\mathbf{z}|\mathbf{x})$ is the single target measurement likelihood, $\kappa_k(\cdot)$ and $\rho_{K,k}(\cdot)$ are the clutter RFS intensity function and cardinality distribution, respectively, $P_j^l = \frac{l!}{(l-j)!}$ is the permutation coefficient with $P_j^l = 0$ when $j > l$ by convention, $e_j(\cdot)$ denotes the elementary symmetric function [25] of order j defined for a finite set Z of real numbers as

$$e_j(Z) = \sum_{S \subseteq Z, |S|=j} \left(\prod_{\zeta \in S} \zeta \right)$$

with $e_0(Z) = 1$ by convention, and $|S|$ is the cardinality of a set S.

For the CPHD filter, the cardinality estimate $\hat{N}_k$ can be obtained by the cardinality function

$$\hat{N}_k = \arg\max_n \rho_k(n). \quad (13)$$

When the cardinalities of the RFS are Poisson-distributed, the PHD recursion can be derived from (4) and (7) (without target spawning):

$$v_{k|k-1}(\mathbf{x}) = \gamma_k(\mathbf{x}) + \int p_{S,k}(\mathbf{x}') f_{k|k-1}(\mathbf{x}|\mathbf{x}') v_{k-1}(\mathbf{x}') d\mathbf{x}' \quad (14)$$

$$v_k(\mathbf{x}) = v_{k|k-1}(\mathbf{x}) \times \left[q_{D,k}(\mathbf{x}) + \sum_{\mathbf{z} \in Z_k} \frac{g_k(\mathbf{z}|\mathbf{x}) p_{D,k}(\mathbf{x})}{\kappa_k(\mathbf{z}) + \langle p_{D,k} g_k(\mathbf{z}|\cdot), v_{k|k-1}\rangle} \right]. \quad (15)$$

The cardinality estimate $\hat{N}_k$ is as follows:

$$\hat{N}_k = \langle v_k, 1\rangle. \quad (16)$$

The implementation method based on the GM model needs pruning and merging to prevent an unbounded increase of the Gaussian components [4], [5].

B. The Inverse Gamma Distribution and Gamma Distribution

The probability density of the inverse gamma (IG) distribution is defined over the support $x > 0$ as

$$\mathrm{IG}(x;\alpha;\beta) = \frac{\beta^\alpha}{\Gamma(\alpha)} x^{-\alpha-1} \exp\left(-\frac{\beta}{x}\right) \quad (17)$$

with shape parameter $\alpha > 0$ and scale parameter $\beta > 0$, and where $\Gamma(\cdot)$ denotes the gamma function. The mode at which the probability density function is the maximum is $\beta/(\alpha+1)$, and the mean value is $\beta/(\alpha-1)$. The variance of the IG distribution is $\beta^2/[(\alpha-1)^2(\alpha-2)]$.

The probability density of the gamma distribution $\mathrm{G}(x;\alpha;\beta)$ is

$$\mathrm{G}(x;\alpha;\beta) = \frac{\beta^\alpha}{\Gamma(\alpha)} x^{\alpha-1} \exp(-\beta x) \quad (18)$$

with shape parameter $\alpha > 0$ and rate parameter $\beta > 0$. Its mode and mean are $(\alpha-1)/\beta$ and α/β, respectively.

III. Analytic Implementation Of The IGGM CPHD And PHD Filters

In this section, the inverse gamma Gaussian mixture (IGGM) CPHD filter and PHD filter will be derived in detail. The nonnegative feature determining the detection probability will be introduced to help the IGGM CPHD and IGGM PHD filters track multiple targets without the detection probability being known a priori. The closed-form solution to the CPHD recursion will be discussed in Section III-A. Section III-B will show the pruning and merging procedure for the IGGM components.

A. IGGM CPHD Filter and IGGM PHD Filter

1) Augmented Target State Transition and Observation Models: In the following, first, the mixture target state and the corresponding measurement are introduced. Then, we present the transition and observation processes of the mixture target state in detail.

Single-target state and measurement: Let the joint single-target state $\mathbf{x}$ contain the positions and velocities $\tilde{\mathbf{x}}$, and the nonnegative feature d, which denotes the SNR throughout, i.e.,

$$\mathbf{x} = [\tilde{\mathbf{x}}, d]^T. \quad (19)$$

We assume that the feature state d and the kinematic state $\tilde{\mathbf{x}}$ are statistically independent and that the single-target detection probability is determined by the feature d, i.e.,

$$p_{D,k}(\mathbf{x}) = p_{D,k}(d). \quad (20)$$

The validity of this assumption mainly comes from the fact that the factor determining the feature is relatively stable in a short time window. For instance, the SNR and echo amplitude for radar and infrared sensors mainly depend on the changes of radar cross section (RCS) and target temperature rather than the small change in target location. Each measurement $\mathbf{z}$ consists of the position measurement $\tilde{\mathbf{z}}$ and the feature measurement h, i.e.,

$$\mathbf{z} = [\tilde{\mathbf{z}}, h]^T. \quad (21)$$

Mixture target intensity: By convention, $\mathcal{N}(\cdot;\mathbf{m};P)$ denotes a Gaussian density with mean $\mathbf{m}$ and covariance P. So, at time k the target density can be denoted by the IGGM as

$$v_k(\tilde{\mathbf{x}}, d) = \sum_{i=1}^{J_k} w_k^{(i)} \mathcal{N}(\tilde{\mathbf{x}}; \mathbf{m}_k^{(i)}; P_k^{(i)}) \mathrm{IG}(d; \alpha_k^{(i)}; \beta_k^{(i)}) \quad (22)$$

where, J_k is the number of the IGGM components. For the ith IGGM component, the estimate of kinematic state $\tilde{\mathbf{x}}$ is $\mathbf{m}_k^{(i)}$. The estimate of feature d is $\beta_k^{(i)}/(\alpha_k^{(i)}-1)$ with an unbiased mean in this paper, or it can be estimated as $\beta_k^{(i)}/(\alpha_k^{(i)}+1)$ with its mode.

Target Markov transition process: The single target survival probability $p_{S,k}(\mathbf{x})$ with kinematic state $\tilde{\mathbf{x}}$, Markov transition density $f_{k|k-1}(\tilde{\mathbf{x}}|\tilde{\mathbf{x}}')$, and measurement likelihood $\tilde{g}_k(\tilde{\mathbf{z}}|\tilde{\mathbf{x}})$ are similar to the standard GM CPHD filter and given by

$$p_{S,k}(\tilde{\mathbf{x}},d)=p_{S,k} \tag{23}$$

$$f_{k|k-1}(\tilde{\mathbf{x}}|\tilde{\mathbf{x}}')=\mathcal{N}(\tilde{\mathbf{x}};F_{k-1}\tilde{\mathbf{x}}';Q_{k-1}) \tag{24}$$

$$\tilde{g}_k(\tilde{\mathbf{z}}|\tilde{\mathbf{x}})=\mathcal{N}(\tilde{\mathbf{z}};H_k\tilde{\mathbf{x}};R_k) \tag{25}$$

where F_{k-1} is the state transition matrix for target, Q_{k-1} is the process noise covariance. Also, H_k and R_k denote the observation matrix, and observation noise covariance, respectively.

The prediction process for the augmented state d is

$$\mathrm{IG}(d;\alpha_{k-1};\beta_{k-1})\rightarrow \mathrm{IG}(d;\alpha_{k|k-1};\beta_{k|k-1}). \tag{26}$$

To maintain the same estimates, the parameters should satisfy

$$\frac{\beta_{k|k-1}}{\alpha_{k|k-1}-1}=\frac{\beta_{k-1}}{\alpha_{k-1}-1}. \tag{27}$$

In this paper, we employ a simple model to describe the non-Gaussian feature prediction process, let $\alpha_{k|k-1}=k_\alpha\alpha_{k-1}$ where $0<k_\alpha<1$. Then, we can obtain $\beta_{k|k-1}=\frac{\beta_{k-1}}{\alpha_{k-1}-1}(k_\alpha\alpha_{k-1}-1)$. This process can preserve (maintain) the estimates and enlarge the predicted variance. To accommodate more complex varying feature process, other methods such as more complex feature translation process model and IMM method can be used. The inverse gamma distribution can approach a Gaussian distribution approximately when the shape parameter has a large value. If $\alpha_{k-1}\gg 1$ and k_α is closer to 1 (slightly increase the variance), let $\delta^2_{k-1,\mathrm{IG}}$ and $\delta^2_{k|k-1,\mathrm{IG}}$ denote the variance before and after the prediction, respectively. Then,

$$\delta^2_{k|k-1,\mathrm{IG}}\approx\frac{1}{k_\alpha}\delta^2_{k-1,\mathrm{IG}}. \tag{28}$$

Observation process: At time k, the likelihood $g_k(h|d)$ for feature d is gamma distributed in the update step. That is,

$$g_k(h|d)=\mathrm{G}\left(h;\xi;\frac{\xi}{d}\right)=\frac{\xi^\xi}{\Gamma(\xi)}d^{-\xi}h^{\xi-1}\exp\left(-\frac{\xi}{d}h\right). \tag{29}$$

The likelihood $g_k(h|d)$ can ensure that the output and predicted features belong to the same family of distribution. The gamma likelihood function is used to describe the non-Gaussian measurement process. In addition, the inverse gamma prior is the conjugate prior of the gamma likelihood distributions. Based on the conjugacy, a closed-form solution can be proposed in this paper.

As the measurements are generated from targets and clutter, $\kappa_k(\mathbf{z})$, the intensity of clutter measurements at time k is determined by both the position measurement and the feature measurement. Thus, based on (21), $\kappa_k(\mathbf{z})$ is also can be denoted as $\kappa_k(\tilde{\mathbf{z}},h)$. It is assumed that the feature of clutter is also IG distribution, i.e.,

$$\kappa_k(\mathbf{z})=\kappa_k(\tilde{\mathbf{z}},h)=\lambda_\kappa c(\tilde{\mathbf{z}})\mathrm{IG}_k^\kappa(d;\alpha_k^\kappa;\beta_k^\kappa)g_k(h|d) \tag{30}$$

where λ_κ is the average clutter intensity, $c(\tilde{\mathbf{z}})$ is clutter position probability density in the measurement space, and $\mathrm{IG}_k^\kappa(d;\alpha_k^\kappa;\beta_k^\kappa)g_k(h|d)$ is the clutter feature probability density in the feature space. The expression $\mathrm{IG}_k^\kappa(d;\alpha_k^\kappa;\beta_k^\kappa)$ denotes the prior distribution of the clutter feature d. The shape parameter α_k^κ and the scale parameter β_k^κ are assumed to be known. The term $g_k(h|d)$ is the likelihood for feature d as (29). Let $\tilde{\kappa}_k(\tilde{\mathbf{z}})=\lambda_\kappa c(\tilde{\mathbf{z}})$.

2) Analytic Implementation: In the IGGM component, the Gaussian distribution denotes the kinematic state $\tilde{\mathbf{x}}$. After the prediction and update steps, the kinematic state $\tilde{\mathbf{x}}$ can keep the same distribution because of the closed-formed solution. The prediction process (26) ensures that the augmented state feature d, which is IG distributed, also maintains the same distribution. In the update step, each IG component is propagated as

$$\begin{aligned}&\mathrm{IG}(d;\alpha_{k|k-1};\beta_{k|k-1})g_k(h|d)=\frac{{\beta_{k|k-1}}^{\alpha_{k|k-1}}}{\Gamma(\alpha_{k|k-1})}d^{-\alpha_{k|k-1}-1}\\&\cdot\exp\left(-\frac{\beta_{k|k-1}}{d}\right)\frac{\xi^\xi}{\Gamma(\xi)}d^{-\xi}h^{\xi-1}\exp\left(-\frac{\xi}{d}h\right)\\&=\frac{{\beta_{k|k-1}}^{\alpha_{k|k-1}}}{\Gamma(\alpha_{k|k-1})}\frac{\xi^\xi}{\Gamma(\xi)}h^{\xi-1}d^{-\xi-\alpha_{k|k-1}-1}\exp\left(-\frac{\beta_{k|k-1}+\xi h}{d}\right).\end{aligned} \tag{31}$$

Given h, (31) is still an IG distribution. Equation (31) can be simplified to

$$\begin{aligned}&\mathrm{IG}(d;\alpha_{k|k-1};\beta_{k|k-1})g_k(h|d)\\&=A\frac{\beta_*^{\alpha_*}}{\Gamma(\alpha_*)}d^{-\alpha_*-1}\exp\left(-\frac{\beta_*}{d}\right)=A\cdot\mathrm{IG}(d;\alpha_*;\beta_*)\end{aligned} \tag{32}$$

where

$$A=\frac{{\beta_{k|k-1}}^{\alpha_{k|k-1}}}{\Gamma(\alpha_{k|k-1})}\frac{\xi^\xi}{\Gamma(\xi)}\frac{\Gamma(\alpha_*)}{\beta_*^{\alpha_*}}h^{\xi-1} \tag{33}$$

$$\alpha_*=\xi+\alpha_{k|k-1} \tag{34}$$

$$\beta_*=\beta_{k|k-1}+\xi h. \tag{35}$$

The new estimate of (31) by an unbiased mean is $\frac{\beta_{k|k-1}+\xi h}{\xi+\alpha_{k|k-1}-1}$, and its value is determined by the measurement, the likelihood function, and the prior distribution. The larger the parameter ξ is, the greater influence the measurement has on the new estimate.

The following two propositions show the prediction and update steps of the IGGM filters.

At time k, the intensity of the birth RFS is an IGGM given by

$$\gamma_k(\tilde{\mathbf{x}},d)=\sum_{i=1}^{J_{\gamma,k}}w_{\gamma,k}^{(i)}\mathcal{N}(\tilde{\mathbf{x}};\mathbf{m}_{\gamma,k}^{(i)};P_{\gamma,k}^{(i)})\mathrm{IG}(d;\alpha_{\gamma,k}^{(i)};\beta_{\gamma,k}^{(i)}) \tag{36}$$

where $J_{\gamma,k}$ is the component number, $w_{\gamma,k}^{(i)}$, $\mathbf{m}_{\gamma,k}^{(i)}$, and $P_{\gamma,k}^{(i)}$ are the weights, means, and covariances of the birth target kinematic state, respectively, $\alpha_{\gamma,k}^{(i)}$ and $\beta_{\gamma,k}^{(i)}$ and are the shapes and scales of the birth target augmented state, respectively.

Proposition 1: If at time $k-1$, the posterior intensity $v_{k-1}(\tilde{\mathbf{x}}, d)$ is an inverse gamma Gaussian mixture of the form given by

$$v_{k-1}(\tilde{\mathbf{x}}, d) = \sum_{i=1}^{J_{k-1}} w_{k-1}^{(i)} \mathcal{N}(\tilde{\mathbf{x}}; \mathbf{m}_{k-1}^{(i)}; P_{k-1}^{(i)}) \mathrm{IG}(d; \alpha_{k-1}^{(i)}; \beta_{k-1}^{(i)}) \tag{37}$$

then, with the known posterior cardinality distribution $\rho_{k-1}(n)$, the predicted intensity is also an inverse gamma Gaussian mixture and the prediction step is given by

$$v_{k-1}(\tilde{\mathbf{x}}, d) = \gamma_k(\tilde{\mathbf{x}}, d) + p_{S,k} \sum_{i=1}^{J_{k-1}} w_{k-1}^{(i)} \mathcal{N}(\tilde{\mathbf{x}}; \mathbf{m}_{k|k-1}^{(i)}; P_{k|k-1}^{(i)}) \mathrm{IG}(d; \alpha_{k|k-1}^{(i)}; \beta_{k|k-1}^{(i)}) \tag{38}$$

$$\rho_{k|k-1}(n) = \sum_{j=0}^{n} \rho_{\Gamma,k}(n-j) \sum_{l=j}^{\infty} C_j^l \rho_{k-1}(l) p_{S,k}^j (1-p_{S,k})^{l-j} \tag{39}$$

where $\gamma_k(\tilde{\mathbf{x}}, d)$ is given in (36),

$$\mathbf{m}_{k|k-1}^{(i)} = F_{k-1} \mathbf{m}_{k-1}^{(i)} \tag{40}$$

$$P_{k|k-1}^{(i)} = F_{k-1} P_{k-1}^{(i)} F_{k-1}^T + Q_{k-1} \tag{41}$$

$$\alpha_{k|k-1}^{(i)} = k_\alpha \alpha_{k-1}^{(i)} \tag{42}$$

$$\beta_{k|k-1}^{(i)} = \frac{\beta_{k-1}^{(i)}}{\alpha_{k-1}^{(i)} - 1} (k_\alpha \alpha_{k-1}^{(i)} - 1). \tag{43}$$

Proposition 2: If at time k, the predicted intensity $v_{k|k-1}(\tilde{\mathbf{x}}, d)$ is an inverse gamma Gaussian mixture of the form given by

$$v_{k|k-1}(\tilde{\mathbf{x}}, d) = \sum_{i=1}^{J_{k|k-1}} w_{k|k-1}^{(i)} \mathcal{N}(\tilde{\mathbf{x}}; \mathbf{m}_{k|k-1}^{(i)}; P_{k|k-1}^{(i)}) \mathrm{IG}(d; \alpha_{k|k-1}^{(i)}; \beta_{k|k-1}^{(i)}) \tag{44}$$

and the predicted cardinality distribution $\rho_{k|k-1}(n)$ is also given, then, with the measurement set Z_k, the updated intensity $v_k(\tilde{\mathbf{x}}, d)$ is also an inverse gamma Gaussian mixture and the update step is given by

$$\begin{aligned} v_k(\tilde{\mathbf{x}}, d) = & \sum_{j=1}^{J_{k|k-1}} (1 - p_{D,k}(d_{k|k-1}^{(j)})) w_{L,k}^{(j)} \\ & \cdot \mathcal{N}(\tilde{\mathbf{x}}; \mathbf{m}_{k|k-1}^{(j)}; P_{k|k-1}^{(j)}) \mathrm{IG}(d; \alpha_{k|k-1}^{(j)}; \beta_{k|k-1}^{(j)}) \\ & + \sum_{\mathbf{z} \in Z_k} \sum_{j=1}^{J_{k|k-1}} w_{D,k}^{(j)}(\mathbf{z}) \mathcal{N}(\tilde{\mathbf{x}}; \mathbf{m}_k^{(j)}; P_k^{(j)}) \mathrm{IG}(d; \alpha_k^{(j)}; \beta_k^{(j)}) \end{aligned} \tag{45}$$

$$\rho_k(n) = \frac{\Upsilon_k^0[v_{k|k-1}, Z_k](n) \rho_{k|k-1}(n)}{\left\langle \Upsilon_k^0[v_{k|k-1}, Z_k], \rho_{k|k-1} \right\rangle} \tag{46}$$

where

$$\Upsilon_k^u[v, Z](n) = \sum_{j=0}^{\min(|Z|,n)} (|Z|-j)! \rho_{K,k}(|Z|-j) P_{j+u}^n \cdot \frac{\left(\sum_{i=1}^{J_{k|k-1}} \left(1 - p_{D,k}(d_{k|k-1}^{(i)})\right) w_{k|k-1}^{(i)}\right)^{n-(j+u)}}{\left(\sum_{i=1}^{J_{k|k-1}} w_{k|k-1}^{(i)}\right)^n} e_j(\Xi_k(v, Z)) \tag{47}$$

$$\Xi_k(v, Z) = \left\{ \sum_{j=1}^{J_{k|k-1}} w_{k|k-1}^{(j)} \psi_{k,\mathbf{z}}^{(j)} : \mathbf{z} \in Z \right\} \tag{48}$$

$$\psi_{k,\mathbf{z}}^{(j)} = \psi_{k,[\tilde{\mathbf{z}},h]^T}^{(j)} = \frac{\langle 1, \kappa_k \rangle}{\kappa_k(\tilde{\mathbf{z}}, h)} q_k^{(j)}(\tilde{\mathbf{z}}) \chi_{v,k}^{(j)}(h) p_{D,k}(d_{k|k-1}^{(j)}) \tag{49}$$

where $\kappa_k(\tilde{\mathbf{z}}, h)$ is the intensity of clutter measurements given by

$$\kappa_k(\tilde{\mathbf{z}}, h) = \tilde{\kappa}_k(\tilde{\mathbf{z}}) \chi_{\kappa,k}(h). \tag{50}$$

And from the Kalman filter, we can obtain

$$q_k^{(j)}(\tilde{\mathbf{z}}) = \mathcal{N}(\tilde{\mathbf{z}}; H_k \mathbf{m}_{k|k-1}^{(j)}; S_{k|k-1}^{(j)}) \tag{51}$$

$$S_{k|k-1}^{(j)} = R_k + H_k P_{k|k-1}^{(j)} H_k^T \tag{52}$$

$$\mathbf{m}_k^{(j)}(\tilde{\mathbf{z}}) = \mathbf{m}_{k|k-1}^{(j)} + K_k^{(j)}(\tilde{\mathbf{z}} - H_k \mathbf{m}_{k|k-1}^{(j)}) \tag{53}$$

$$P_k^{(j)} = [I - K_k^{(j)} H_k] P_{k|k-1}^{(j)} \tag{54}$$

$$K_k^{(j)} = P_{k|k-1}^{(j)} H_k^T [S_{k|k-1}^{(j)}]^{-1}. \tag{55}$$

From (33), we can obtain two coefficients as follows:

$$\chi_{v,k}^{(j)}(h) = \frac{\left(\beta_{k|k-1}^{(j)}\right)^{\alpha_{k|k-1}^{(j)}}}{\Gamma(\alpha_{k|k-1}^{(j)})} \frac{h^{\xi_k - 1}}{\Gamma(\xi_k)} {\xi_k}^{\xi_k} \frac{\Gamma(\alpha_{k|k-1}^{(j)} + \xi_k)}{\left(\beta_{k|k-1}^{(j)} + h\xi_k\right)^{\alpha_{k|k-1}^{(j)} + \xi_k}} \tag{56}$$

$$\chi_{\kappa,k}(h) = \frac{(\beta_k^\kappa)^{\alpha_k^\kappa}}{\Gamma(\alpha_k^\kappa)} \frac{h^{\xi_k - 1}}{\Gamma(\xi_k)} {\xi_k}^{\xi_k} \frac{\Gamma(\xi_k + \alpha_k^\kappa)}{(\beta_k^\kappa + \xi_k h)^{\xi_k + \alpha_k^\kappa}}. \tag{57}$$

Also, $d_{k|k-1}^{(j)} = \frac{\beta_{k|k-1}^{(j)}}{\alpha_{k|k-1}^{(j)} - 1}$ denotes the feature estimates in the prediction step. Finally, $w_{L,k}^{(j)}$ and $w_{D,k}^{(i)}(\mathbf{z})$ are the weights of the missed detection and observed detection whose values are as follows:

$$w_{L,k}^{(j)} = w_{k|k-1}^{(j)} \frac{\left\langle \Upsilon_k^1[v_{k|k-1}, Z_k], \rho_{k|k-1} \right\rangle}{\left\langle \Upsilon_k^0[v_{k|k-1}, Z_k], \rho_{k|k-1} \right\rangle} \tag{58}$$

$$w_{D,k}^{(i)}(\mathbf{z}) = \psi_{k,\mathbf{z}}^{(j)} \frac{\left\langle \Upsilon_k^1[v_{k|k-1}, Z_k - \{\mathbf{z}\}], \rho_{k|k-1} \right\rangle}{\left\langle \Upsilon_k^0[v_{k|k-1}, Z_k], \rho_{k|k-1} \right\rangle}. \tag{59}$$

To set up the proposition 2, we have to assume that the detection probability of each target is relatively constant around the mean of the IG function or the IG distribution is approximating to Dirac delta function. The proofs are shown in Appendix A.

When the cardinalities of the RFS are Poisson-distributed, the IGGM PHD recursion can be derived from (38) and (45) (without target spawning). The prediction is given in (38), and the update is given by

$$\begin{aligned} & v_k(\tilde{\mathbf{x}}, d) \\ &= \sum_{\mathbf{z}\in Z_k} \sum_{j=1}^{J_{k|k-1}} w_{C,k}^{(j)}(\mathbf{z}) \mathcal{N}(\tilde{\mathbf{x}}; \mathbf{m}_k^{(j)}; P_k^{(j)}) \mathrm{IG}(d; \alpha_k^{(j)}; \beta_k^{(j)}) \\ &+ \sum_{j=1}^{J_{k|k-1}} (1 - p_{D,k}(d_{k|k-1}^{(j)})) w_{k|k-1}^{(j)} \\ &\cdot \mathcal{N}(\tilde{\mathbf{x}}; \mathbf{m}_{k|k-1}^{(j)}; P_{k|k-1}^{(j)}) \mathrm{IG}(d; \alpha_{k|k-1}^{(j)}; \beta_{k|k-1}^{(j)}) \end{aligned} \tag{60}$$

where

$$\begin{aligned} & w_{C,k}^{(j)}(\mathbf{z}) = w_{C,k}^{(j)}(\tilde{\mathbf{z}}, h) \\ &= \frac{p_{D,k}(d_{k|k-1}^{(j)}) w_{k|k-1}^{(j)} q_k^{(j)}(\tilde{\mathbf{z}}) \chi_{v,k}^{(j)}(h)}{\kappa_k(\tilde{\mathbf{z}}, h) + \sum_{l=1}^{J_{k|k-1}} p_{D,k}(d_{k|k-1}^{(l)}) w_{k|k-1}^{(l)} q_k^{(l)}(\tilde{\mathbf{z}}) \chi_{v,k}^{(l)}(h)}. \end{aligned} \tag{61}$$

State extraction in the IGGM CPHD filter and IGGM PHD filter involves estimating the number of targets and extracting the corresponding number of mixture components. The procedures for extracting the kinematic state are similar to those in the standard GM CPHD filter and GM PHD filter. The feature d is the mean value of the corresponding IG component.

The complexity of the IGGM CPHD filter is $O\left(nm^3\right)$, which has the same order as that of the standard CPHD filter [2] where m and n denote the cardinalities of the measurements and targets, respectively. It can be reduced to $O\left(nm^2\log^2 m\right)$ by decomposition and recursion [4]. Meanwhile, the IGGM PHD filter and the standard PHD filter have the same order complexity, which is substantially less than that of the corresponding CPHD filters.

In the IGGM filters, we make the similar assumption that the clutter parameters and target birth model are known a priori like the standard GM filters. In practice, the clutter generator model [7]–[9] may be used to handle the unknown clutter parameters case and the measurements-driven method may accommodate the unknown target birth model [14]–[17].

B. Merging Inverse Gamma Gaussian Mixture Components

The IGGM CPHD filter and IGGM PHD filter also need their mixture components to be pruned and merged, to prevent unbounded growth. The pruning procedure is similar to that in the standard GM CPHD filter, where mixture components with weak weights are discarded [4], [5]. The merging procedure combines similar components into one. The IGGM components can be split into inverse gamma components and Gaussian components, as each IGGM component is variable-separable. Inspired by [26], which merged gamma Gaussian mixture components, the merging procedure for the inverse gamma Gaussian mixture components is introduced as follows.

1) Merging Criterion: Suppose that at time k there are two IGGM components $\Psi(\tilde{\mathbf{x}}, d)$ and $\Omega(\tilde{\mathbf{x}}, d)$:

$$\begin{aligned} \Psi(\tilde{\mathbf{x}}, d) &= w_k^{(\Psi)} \mathcal{N}(\tilde{\mathbf{x}}; \mathbf{m}_k^{(\Psi)}; P_k^{(\Psi)}) \mathrm{IG}(d; \alpha_k^{(\Psi)}; \beta_k^{(\Psi)}) \\ &= w_k^{(\Psi)} \mathcal{N}_\Psi(\tilde{\mathbf{x}}) \mathrm{IG}_\Psi(d) \end{aligned} \tag{62}$$

$$\begin{aligned} \Omega(\tilde{\mathbf{x}}, d) &= w_k^{(\Omega)} \mathcal{N}(\tilde{\mathbf{x}}; \mathbf{m}_k^{(\Omega)}; P_k^{(\Omega)}) \mathrm{IG}(d; \alpha_k^{(\Omega)}; \beta_k^{(\Omega)}) \\ &= w_k^{(\Omega)} \mathcal{N}_\Omega(\tilde{\mathbf{x}}) \mathrm{IG}_\Omega(d). \end{aligned} \tag{63}$$

To merge the two components, we first need to determine whether they are similar to each other. Due to the assumed conditional independence of the distributions over $\tilde{\mathbf{x}}$ and d, the distances $\mathrm{Dis}_{\mathrm{GM}}(\mathcal{N}_\Psi(\tilde{\mathbf{x}}), \mathcal{N}_\Omega(\tilde{\mathbf{x}}))$ and $\mathrm{Dis}_{\mathrm{IG}}(\mathrm{IG}_\Psi(d), \mathrm{IG}_\Omega(d))$ denote the degree to which the two Gaussian distributions are similar to each other and the two inverse gamma distributions are similar to each other, respectively. If $\mathrm{Th}_{\mathrm{GM}}$ and $\mathrm{Th}_{\mathrm{IG}}$ are the merging thresholds for Gaussian components and IG components, respectively, the merging criterion is

$$(\mathrm{Dis}_{\mathrm{GM}} < \mathrm{Th}_{\mathrm{GM}}) \,\&\, (\mathrm{Dis}_{\mathrm{IG}} < \mathrm{Th}_{\mathrm{IG}}) \tag{64}$$

where $\mathrm{Dis}_{\mathrm{GM}} = \mathrm{Dis}_{\mathrm{GM}}(\mathcal{N}_\Psi(\tilde{\mathbf{x}}), \mathcal{N}_\Omega(\tilde{\mathbf{x}}))$ as given in [4], & is the logical "AND" operator, and $\mathrm{Dis}_{\mathrm{IG}} = \mathrm{Dis}_{\mathrm{IG}}(\mathrm{IG}_\Psi(d), \mathrm{IG}_\Omega(d))$. The calculation of $\mathrm{Dis}_{\mathrm{IG}}$ is described as follows.

The Kullback-Leibler divergence $\mathrm{KL}(p||q)$ is used to describe the similarity between two distributions [26]–[28], where

$$\mathrm{KL}(p||q) = \int p(x) \log\left(\frac{p(x)}{q(x)}\right) dx \tag{65}$$

and $p(x)$ and $q(x)$ are two distributions in the same space. The more similar $p(x)$ and $q(x)$ are, the smaller $\mathrm{KL}(p||q)$ is. Therefore, Kullback-Leibler divergence can be used to calculate $\mathrm{Dis}_{\mathrm{IG}}$. Because $\mathrm{KL}(p||q) \neq \mathrm{KL}(q||p)$, the expression for $\mathrm{Dis}_{\mathrm{IG}}(\mathrm{IG}_\Psi(d), \mathrm{IG}_\Omega(d))$ is given by

$$\mathrm{Dis}_{\mathrm{IG}}(\mathrm{IG}_\Psi(d), \mathrm{IG}_\Omega(d)) = \mathrm{KL}(\mathrm{IG}_p||\mathrm{IG}_q) + \mathrm{KL}(\mathrm{IG}_q||\mathrm{IG}_p). \tag{66}$$

Let $p(x)$ and $q(x)$ denote two IG distributions

$$p(x) = \mathrm{IG}(x; \alpha_1; \beta_1) \tag{67}$$

$$q(x) = \mathrm{IG}(x; \alpha_2; \beta_2). \tag{68}$$

Then, the corresponding $\mathrm{KL}(p||q)$ can be calculated as follows:

$$\begin{aligned} & \mathrm{KL}(p||q) = \int p(x) \log\left(\frac{p(x)}{q(x)}\right) dx \\ &= \int p(x) \log(p(x)) dx - \int p(x) \log(q(x)) dx \\ &= \log\left(\frac{\beta_1^{\alpha_1}}{\Gamma(\alpha_1)}\right) \int p(x) dx - \log\left(\frac{\beta_2^{\alpha_2}}{\Gamma(\alpha_2)}\right) \int p(x) dx \\ &- (\alpha_1 + 1) \int p(x) \log(x) dx - \beta_1 \int p(x) \frac{1}{x} dx \\ &+ (\alpha_2 + 1) \int p(x) \log(x) dx + \beta_2 \int p(x) \frac{1}{x} dx. \end{aligned} \tag{69}$$

Since $\int p(x) \log(x) dx = \log \beta_1 - \varphi_0(\alpha_1)$and $\int p(x) \frac{1}{x} dx = \frac{\alpha_1}{\beta_1}$ (proofs are given in the Appendix B), where $\varphi_0(\cdot)$ is the

digamma function or the 0-order polygamma function, (69) is simplified to

$$\mathrm{KL}(p||q) = \log\left(\frac{\beta_1^{\alpha_1}}{\Gamma(\alpha_1)}\right) - \log\left(\frac{\beta_2^{\alpha_2}}{\Gamma(\alpha_2)}\right) + \beta_2\frac{\alpha_1}{\beta_1} - \alpha_1 + (\alpha_2 - \alpha_1)\left(\log\beta_1 - \varphi_0(\alpha_1)\right). \quad (70)$$

The derivation of $\mathrm{KL}(q||p)$ is similar to that of $\mathrm{KL}(p||q)$. Thus $\mathrm{Dis}_{\mathrm{IG}}(p(x), q(x))$ is given by

$$\begin{aligned}\mathrm{Dis}_{\mathrm{IG}}(p(x), q(x)) &= \mathrm{KL}(p||q) + \mathrm{KL}(q||p)\\ &= (\alpha_1 - \alpha_2)\left(\varphi_0(\alpha_1) - \varphi_0(\alpha_2) + \log\frac{\beta_2}{\beta_1}\right)\\ &\quad + (\beta_1 - \beta_2)\left(\frac{\alpha_2}{\beta_2} - \frac{\alpha_1}{\beta_1}\right) \quad (71)\end{aligned}$$

and $\mathrm{Dis}_{\mathrm{IG}}(\mathrm{IG}_\Psi(d), \mathrm{IG}_\Omega(d))$ is given by

$$\begin{aligned}&\mathrm{Dis}_{\mathrm{IG}}(\mathrm{IG}_\Psi(d), \mathrm{IG}_\Omega(d))\\ &= (\alpha_k^{(\Psi)} - \alpha_k^{(\Omega)})\left(\varphi_0(\alpha_k^{(\Psi)}) - \varphi_0(\alpha_k^{(\Omega)}) + \log\frac{\beta_k^{(\Omega)}}{\beta_k^{(\Psi)}}\right)\\ &\quad + (\beta_k^{(\Psi)} - \beta_k^{(\Omega)})\left(\frac{\alpha_k^{(\Omega)}}{\beta_k^{(\Omega)}} - \frac{\alpha_k^{(\Psi)}}{\beta_k^{(\Psi)}}\right). \quad (72)\end{aligned}$$

2) Merged Distribution: Having given the merging criterion and the derivation of $\mathrm{Dis}_{\mathrm{IG}}(\mathrm{IG}_\Psi(d), \mathrm{IG}_\Omega(d))$, we will now show how to merge several IG components into one. In (65), $p(x)$ denotes a series of IG components and $q(x)$ is the merged IG component. Then,

$$p(x) = \sum_{i=1}^{N} w_i p_i(x) = \sum_{i=1}^{N} w_i \mathrm{IG}(x; \alpha_i; \beta_i) \quad (73)$$

$$q(x) = \tilde{w}\mathrm{IG}(x; \alpha; \beta) \quad (74)$$

where $\tilde{w} = \sum_{i=1}^{N} w_i$, which can be obtained by matching the expected values of $p(x)$ and $q(x)$. Note that computing the optimal $q(x)$ to approximate to $p(x)$ is equivalent to minimizing $\mathrm{KL}(p||q)$. That is,

$$\begin{aligned}\min_q(\mathrm{KL}(p||q)) &= \max_q\left(\int p(x)\log(q(x))dx\right)\\ &= \max_q\left(\sum_{i=1}^{N} w_i \int p_i(x)\log(q(x))dx\right). \quad (75)\end{aligned}$$

Let $f(x) = \sum_{i=1}^{N} w_i \int p_i(x)\log(q(x))dx$, and using

$$\begin{aligned}&\int p_i(x)\log(q(x))dx\\ &= \log\left(\frac{\beta^\alpha}{\Gamma(\alpha)}\right) - (\alpha+1)\left(\log\beta_i - \varphi_0(\alpha_i)\right) - \beta\frac{\alpha_i}{\beta_i}, \quad (76)\end{aligned}$$

$f(x)$ can be written as

$$\begin{aligned}f(x) &= \tilde{w}\log\left(\frac{\beta^\alpha}{\Gamma(\alpha)}\right)\\ &\quad + (\alpha+1)\sum_{i=1}^{N}\left(\log\beta_i - \varphi_0(\alpha_i)\right) - \beta\sum_{i=1}^{N}\frac{\alpha_i}{\beta_i}. \quad (77)\end{aligned}$$

Taking the derivative of $f(x)$ with respect to β, equating the result to 0 and solving for β, we obtain

$$\beta = \tilde{w}\alpha \Big/ \sum_{i=1}^{N} w_i\frac{\alpha_i}{\beta_i}. \quad (78)$$

Taking the derivative of $f(x)$ with respect to α and equating the result to 0, we get

$$0 = \sum_{i=1}^{N} w_i(\log\beta - \varphi_0(\alpha) - \log\beta_i + \varphi_0(\alpha_i)). \quad (79)$$

Substituting (78) into (79) and simplifying the result, we get

$$\begin{aligned}0 &= \log\alpha - \varphi_0(\alpha)\\ &\quad + \frac{1}{\tilde{w}}\sum_{i=1}^{N} w_i(\varphi_0(\alpha_i) - \log\beta_i) - \log\left(\frac{1}{\tilde{w}}\sum_{i=1}^{N} w_i\frac{\alpha_i}{\beta_i}\right). \quad (80)\end{aligned}$$

The parameter can be obtained using Newton's algorithm [29].

IV. Results

In this section, the proposed CPHD and PHD filters are tested on a real high-clutter scenario in Section IV-A and simulated scenarios in Section IV-B.

A. Real Scenario

The real sequence consists of 78 frames of long wave infrared (LWIR) data consisting of an F1 Mirage fighter jet obtained in July 1996 in Crete, Greece [30]. The 920×480 pixel frames, which are taken at a rate of 1 Hz, have been registered to compensate for frame-to-frame jitter. The target appears late in the real scenario and moves towards the sensor. There are about 600 detections per frame due to false alarms or clutter. This sequence is a benchmark problem for track initialization and target tracking in heavy clutter with unknown target probability of detection. The best performances are obtained by expectation-maximization method combined with maximum likelihood estimator and maximum likelihood estimator combined with probabilistic data associatior method whose acronyms are EM-ML and ML-PDA respectively [31], [32], however, they are not the recursive algorithms and are unable to give instantaneous estimates. In this paper, two commonly used recursive algorithms that can operate under low SNR conditions in heavy clutter, namely, IMM-MHT and IMM-PDA [33], [34], are used for comparison. A sample frame is illustrated in Fig. 1 where position measurements and SNR (dB) are shown.

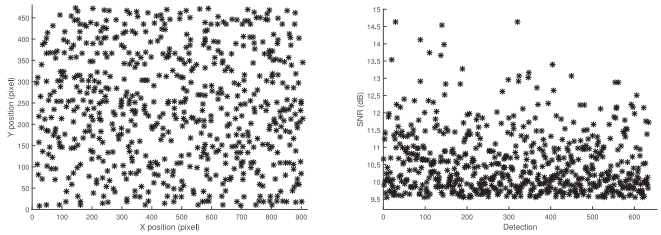

(a) (b)

Fig. 1. The 40th frame of measurements. (a) position (b) SNR.

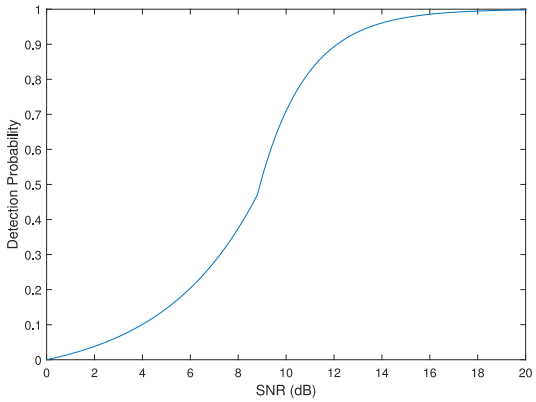

Fig. 2. The detection probability when $\mathrm{SNR}_{th} = 8.8$.

Suppose that the target detection is given by

$$p_{D,k}(d) = \begin{cases} \varepsilon_1 \cdot (\exp((d - \mathrm{SNR}_{th})/\delta_1) - \varepsilon_2) & d < \mathrm{SNR}_{th} \\ \varepsilon_1 \cdot (2 - \exp(-(d - \mathrm{SNR}_{th})/\delta_2) - \varepsilon_2) & d \geq \mathrm{SNR}_{th} \end{cases} \tag{81}$$

where SNR_{th} is 8.8 while δ_1 and δ_2 influence target detection probability in terms of feature d. In this experiment, $\delta_1 = 4$ and $\delta_2 = 2$. In the above, ε_1 is normalizing constant, which is given by $\varepsilon_1 = (2 - \exp(-\mathrm{SNR}_{th}/\delta_1))^{-1}$, and $\varepsilon_2 = \exp(-\mathrm{SNR}_{th}/\delta_1)$. The detection probability specified by (81) is illustrated in Fig. 2, which shows that the assumption in proposition 2 is not supported well. The constant velocity (CV) motion model is used to model the target. The standard deviations of the process noise and measurement noise are 0.5 pixel$\cdot s^{-2}$ and 1 pixel, respectively. In the prediction step (26), k_α is 0.9. The value of parameter ξ in the likelihood function $g_k(h|d)$ for feature d is 5. For the clutter model, we assume $\alpha_k^\kappa = 26$ and $\beta_k^\kappa = 225$. From Fig. 1, we can see that the selected parameters do not match the real SNR and clutter distribution. To accommodate the unknown target birth model, the proposed method and their standard counterparts are integrated with PUB model [17], whose expected number of new targets w_k^b is set to 0.5. For the GM filters, the detection probability is fixed to an appropriate value of 0.7 [32], [33], and for the IGGM filters, the variance of the IG distribution is 9. The parameters are summarized in Table I.

The results produced by the standard GM PHD, GM CPHD, proposed IGGM CPHD and IGGM PHD filters are shown in Fig. 3. It can be seen that the four filters provide the similar

TABLE I
THE PARAMETERS USED IN REAL SCENARIO

Parameter	k_α	ξ	α_k^κ	β_k^κ	w_k^b
Value	0.9	5	26	225	0.5

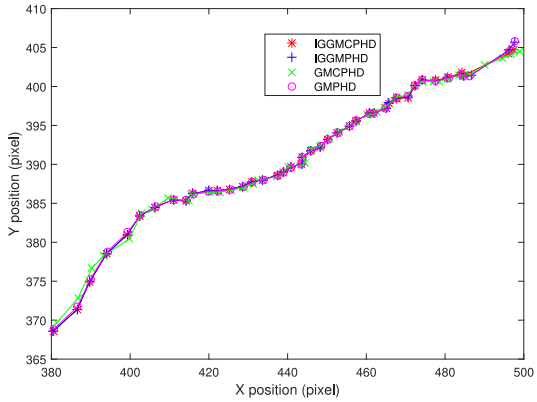

Fig. 3. The confirmed trajectory.

TABLE II
FRAMES USED TO CONFIRM THE TRAJECTORY

Method	IMM MHT	IMM PDA	GM CPHD
Frame Number	38	39	32
Method	GM PHD	IGGM CPHD	IGGM PHD
Frame Number	32	32	31

position estimates indicating that the proposed filters can track the only target with unknown detection probability well in heavy clutter and mismatch of clutter parameters. Track confirmation times for different methods are given in Table II. It shows that the track confirmation occurs at frame 32 by the proposed methods and their standard counterparts in contrast to frames 38 and 39 by IMM-MHT and IMM-PDA methods as reported in [33], [34]. That is, the target is confirmed 6s earlier by the proposed methods. This experiment also shows that the robustness of the proposed filters with mismatched parameters and unstable detection probability, also, the two proposed filters can handle the unknown target birth case with PUB model.

B. Simulated Scenarios

In this section, simulations will be used to assess the performance of the proposed CPHD and PHD filters quantitatively. Section IV-B 1) utilizes a linear Gaussian example to demonstrate the multitarget tracking performance of the IGGM CPHD and PHD filters. Section IV-B 2) examines the nonlinear motion multitarget tracking performance of the IGGM filters. The optimal sub-pattern assignment (OSPA) metric interpreted as per-target error [35] with parameters $p = 1$ and $c = 300$ m will be employed as the main performance metric. A smaller OSPA means less estimation error and hence better performance. In this section, the pruning procedure is performed at each step using a weight threshold $T = 10^{-5}$; the merging thresholds for Gaussian components and IG components are $\mathrm{Th}_{\mathrm{GM}} = 4$ m

TABLE III
THE INITIAL TARGET STATES

	Kinematic state	Feature	Survival time
Target 1	$[-800, -200, 20, -5]^T$	10	$[1, 40]s$
Target 2	$[-800, -200, 12.5, 7]^T$	10	$[1, 40]s$
Target 3	$[-200, 800, 16, 9.7]^T$	10	$[50, 100]s$
Target 4	$[-200, 800, -2.5, -14.6]^T$	10	$[50, 100]s$
Target 5	$[0, 0, 0, -10]^T$	10	$[20, 80]s$
Target 6	$[400, -600, -10.5, 5]^T$	10	$[20, 80]s$

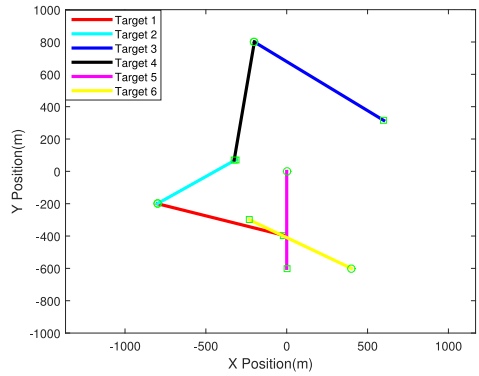

Fig. 4. The confirmed trajectory.

and $\mathrm{Th_{IG}} = 0.05$, and the maximum of the mixture components is $J_{max} = 100$. The cardinality distribution is capped at $N_{max} = 100$ terms.

1) Simulation for Examining the Validity of the IGGM Filters: There are six targets in the surveillance region $[-1000, 1000]$ m $\times$ $[-1000, 1000]$ m. Each target follows the nearly-constant velocity motion model and its kinematic state vector includes the position and velocity $\tilde{\mathbf{x}}_k = [p_{x,k}, p_{y,k}, \dot{p}_{x,k}, \dot{p}_{y,k}]^T$. Each measurement vector includes the position and feature measurement $\mathbf{z}_k = [\tilde{\mathbf{z}}_k, h]^T$, where $\tilde{\mathbf{z}}_k = [z_{x,k}, z_{y,k}]^T$. The parameters in (24) and (25) are given as

$$F_k = \begin{bmatrix} I_2 & \delta t I_2 \\ 0_2 & I_2 \end{bmatrix} \quad Q_k = \sigma_v^2 \begin{bmatrix} \frac{\delta t^4}{4} I_2 & \frac{\delta t^3}{2} I_2 \\ \frac{\delta t^3}{2} I_2 & \delta t^2 I_2 \end{bmatrix}$$

$$H_k = \begin{bmatrix} I_2 & 0_2 \end{bmatrix} \quad R_k = \sigma_\varepsilon^2 I_2$$

where I_n and 0_n denote the $n \times n$ identity and zero matrices, respectively, $\delta t = 1$ s is the sampling period, while $\sigma_v = 5$ ms^{-2} and $\sigma_\varepsilon = 10$ m are the standard deviations of the process noise and measurement noise, respectively. In the prediction step (26), k_α is 0.9. The parameter ξ in likelihood function $g_k(h|d)$ for feature d is 5. Suppose that the target detection probability $p_{D,k}(d)$ follows (81) and $\delta_1 = 4$ and $\delta_2 = 2$. In the simulation, the survival probability is $p_{S,k} = 0.99$. Other parameters are the same as in Section V-A. The initial states are shown in Table III, and the true trajectories are shown in Fig. 4.

Fixed detection probability: In this simulation, the initial values of feature d for the six targets are fixed as shown in Table III. The target birth process is a Poisson RFS with intensity

$$\gamma_k(\tilde{\mathbf{x}}, d) = \sum_{i=1}^{4} w_\gamma \mathcal{N}(\tilde{\mathbf{x}}; \mathbf{m}_\gamma^{(i)}; P_\gamma) \mathrm{IG}(d; \alpha_\gamma^{(i)}; \beta_\gamma^{(i)}) \quad (82)$$

TABLE IV
THE PARAMETERS USED IN FIXED DETECTION PROBABILITY SCENARIO

Parameter	σ_v	σ_ε	k_α	ξ	$p_{S,k}$	k_{Be}
Value	$5ms^{-2}$	$10m$	0.9	5	0.99	1.02
Parameter	$\alpha_\gamma^{(i)}$	$\beta_\gamma^{(i)}$	α_k^κ	β_k^κ	λ_κ	
Value	51	500	31	280	$1.25 \times 10^{-5} m^{-2}$	

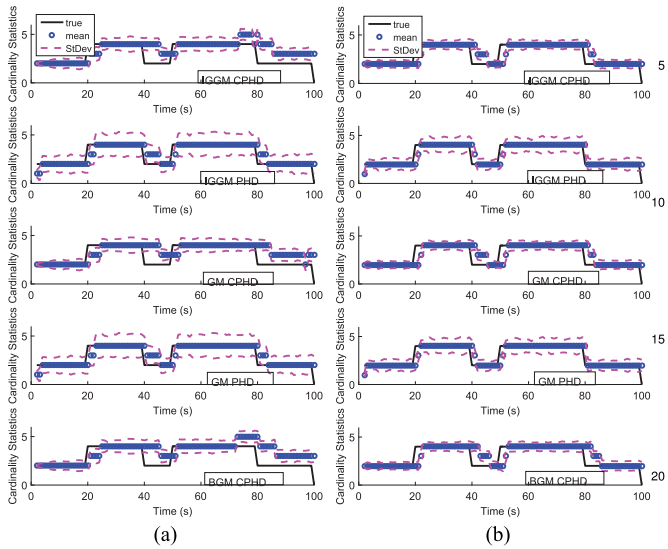

Fig. 5. Average of cardinality estimates in 50 Monte Carlo runs. (a) $\mathrm{SNR}_{th} = 9$, $p_{D,k} = 0.68$. (b) $\mathrm{SNR}_{th} = 5.5$, $p_{D,k} = 0.94$.

where $w_\gamma = 0.03$, $\mathbf{m}_\gamma^{(1)} = [-800, -200, 0, 0]^T$, $\mathbf{m}_\gamma^{(2)} = [-200, 800, 0, 0]^T$, $\mathbf{m}_\gamma^{(3)} = [0, 0, 0, 0]^T$, $\mathbf{m}_\gamma^{(4)} = [400, -600, 0, 0]^T$, $P_\gamma = diag([100, 100, 100, 100]^T)$, $\alpha_\gamma^{(i)} = 51$, and $\beta_\gamma^{(i)} = 500$, so the mean estimate of feature d is 10. Clutter is also a Poisson RFS whose intensity is $\kappa_k(\tilde{\mathbf{z}}, h) = \lambda_\kappa c(\tilde{\mathbf{z}}) \mathrm{IG}_k^\kappa(d; \alpha_k^\kappa; \beta_k^\kappa) g_k(h|d)$, where the average clutter intensity $\lambda_\kappa = 1.25 \times 10^{-5} m^{-2}$, $c(\tilde{\mathbf{z}}) = Vu(\tilde{\mathbf{z}})$, $V = 4 \times 10^6$ m^2 is the "volume" of the region, and $u(\tilde{\mathbf{z}})$ is the uniform probability density. Hence, there are 50 false detections per frame. The parameters in $\mathrm{IG}_k^\kappa(d; \alpha_k^\kappa; \beta_k^\kappa)$ are $\alpha_k^\kappa = 31$ and $\beta_k^\kappa = 280$. In this simulation, suppose that the SNR_{th} in (81) has two different values: 9 and 5.5. The corresponding detection probabilities are 0.68 and 0.94. The two different detection probabilities are known a priori to the standard GM CPHD filter, GM PHD filter. Besides the two standard GM filters, The Beta Gaussian Mixture (BGM) CPHD filter, which is the only CPHD filter in the literature to track an unknown detection probability target, is also employed as a compared tracker. Let $\mathrm{Be}(a; s_\gamma; t_\gamma)$ denote a Beta distribution with parameters $s_\gamma > 1$ and $t_\gamma > 1$. In the BGM CPHD filter, the Beta component, denoting the detection probability, is initialized with $s_\gamma = 68$, $t_\gamma = 32$ and $s_\gamma = 94$, $t_\gamma = 6$, matching with the true detection probabilities. In addition, the prescribed factor $k_{\mathrm{Be}} = 1.02$. The parameters are summarized in Table IV.

The average results over 50 Monte Carlo runs for the two different detection probabilities are shown in Figs. 5 and 6, corresponding to the performance metrics on the number of targets and their locations estimation accuracy. In Fig. 5, the black curve denotes the true target number at each frame; the blue circle is

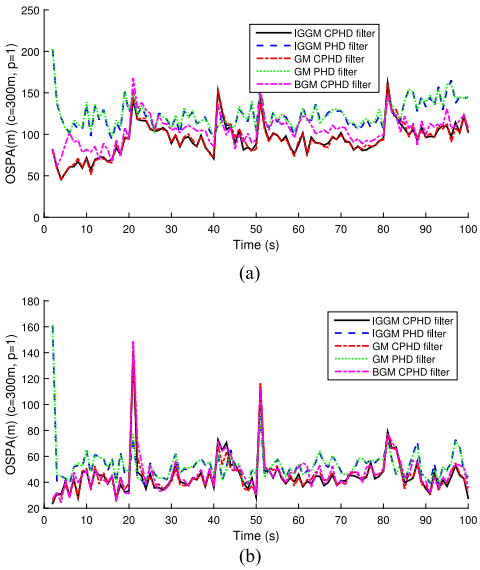

Fig. 6. Average of OSPA distances in 50 Monte Carlo runs. (a) $\mathrm{SNR}_{th} = 9$, $p_{D,k} = 0.68$. (b) $\mathrm{SNR}_{th} = 5.5$, $p_{D,k} = 0.94$.

TABLE V
AVERAGE COMPUTATIONAL TIMES

SNR_{th}	IGGM CPHD	IGGM PHD	GM CPHD	GM PHD	BGM CPHD
9	34.2s	16.7s	30.8s	7.1s	33.9s
5.5	17.7s	1.1s	17.1s	0.9s	17.9s

TABLE VI
DETECTION PROBABILITY RANGES FOR DIFFERENT TARGETS

SNR_{th}	Target 1	Target 2	Target 3
4	$[0.935, 0.986]$	$[0.863, 0.993]$	$[0.775, 0.97]$
5.5	$[0.872, 0.971]$	$[0.73, 0.99]$	$[0.554, 0.94]$
SNR_{th}	Target 4	Target 5	Target 6
4	$[0.863, 0.95]$	$[0.825, 0.986]$	$[0.917, 0.999]$
5.5	$[0.73, 0.9]$	$[0.653, 0.971]$	$[0.836, 0.997]$

the average estimate number of targets and the pink curve denotes the standard deviation of the estimated target cardinality. We can observe that the three CPHD filters overestimate the target cardinality when the detection probabilities are fixed to 0.68. Comparing with the GM CPHD filter, in all frames the IGGM CPHD filter produces cardinality estimate bias in only 6 frames, while for BGM CPHD filter, the frame number is 8. However, when the detection probabilities increase to a higher value, all five filters converge to the correct number of targets. The standard deviation range (StDev) values shown in Fig. 5(b) indicate that the IGGM PHD filter has a larger variance of cardinality estimates than the IGGM CPHD filter, and the two GM filters also show the same results. That means the PHD filters cardinality estimate is jumpy and less stable as a result. Fig. 5 also shows that the PHD filters responds faster to changes in cardinality. In Fig. 6, note that the proposed IGGM filters shows a multitarget tracking performance that is similar to the standard GM filters with exactly known probability with the similar OSPA distance with both low and high fixed detection probability scenarios. The BGM CPHD with correct initial detection probability yields slightly higher location error, especially in the low probability scenario. In contrast, the IGGM PHD and GM PHD filters have a larger OSPA distance than the three CPHD filters, and thus the two PHD filters have a larger estimation error. A possible explanation is that, as expected, the PHD filters cardinality estimates are jumpy and fluctuant when compared with those of the CPHD filter. This simulation shows that the IGGM CPHD filter outperforms the BMG CPHD filter with low detection probability, and the two IGGM filters with unknown detection probability can achieve multitarget tracking performance similar to their standard counterparts with exactly known detection probability.

The complexity is illustrated by comparing the computation time on an Intel Core 3.40 GHz CPU PC with 8 GB RAM and MATLAB R2014b. Based on 50 Monte Carlo runs, the average computational times of the five filters are shown in Table V. It can be seen that the IGGM filters is only a little more computationally expensive than the standard GM filters in high detection probability scenario, and with the detection probability decreasing, the IGGM filters costs more computationally to tackle the unknown target detection probability situation.

Changing detection probability: In this simulation, the initial feature d for the six targets are 10, 10, 8, 8, 9, and 12; the feature values belong to those of a sine function; the amplitudes are 1.5, 3, 2, 1, 2.5, and 4. The periods of the sine functions are $40\delta t$. The parameter α_γ^i in (82) is 51, and parameter β_γ^i is 500, 400, 450, and 600 with respect to differences in i. The parameter SNR_{th} has two values: 4 and 5.5 corresponding to high detection probability and low detection probability cases. The detection probability ranges for different targets are shown in Table VI. The standard GM filters and the BGM CPHD filters are employed to demonstrate the proposed filters performance. We assume that the detection probability for the GM CPHD filter is 0.85 and 0.95. The Beta distribution $\mathrm{Be}(a; s_\gamma; t_\gamma)$ has two sets of initial parameters to accommodate the two different detection probability cases. The parameters of the first group are $[s_\gamma^{(1)} = 97\ t_\gamma^{(1)} = 3,\ s_\gamma^{(2)} = 92\ t_\gamma^{(2)} = 8,\ s_\gamma^{(3)} = 95\ t_\gamma^{(3)} = 5,\ s_\gamma^{(4)} = 99\ t_\gamma^{(4)} = 1]$, while the parameters of the second group are $[s_\gamma^{(1)} = 94\ t_\gamma^{(1)} = 6,\ s_\gamma^{(2)} = 84\ t_\gamma^{(2)} = 16,\ s_\gamma^{(3)} = 90\ t_\gamma^{(3)} = 10,\ s_\gamma^{(4)} = 98\ t_\gamma^{(4)} = 2]$. Other parameters are the same as those in the fixed probability simulation scenario.

The average cardinality estimates with 50 Monte Carlo runs are shown in Fig. 7. Remarkably, both proposed filters can estimate the correct target cardinality when the detection probability is unknown and changing. However, for the higher detection probability case, the GM CPHD filter with $p_{D,k} = 0.85$ produces obvious cardinality estimation errors between 25 s and 88 s, as shown in Fig. 7(a). In Fig. 7(b), when SNR_{th} is 5.5, the lower detection probability leads to inferior results except with GM CPHD with $p_{D,k} = 0.85$. The tracking performance of GM CPHD with $p_{D,k} = 0.85$ improves owning to the appropriate $p_{D,k}$, but it still produces some bias. Both the GM CPHD filter

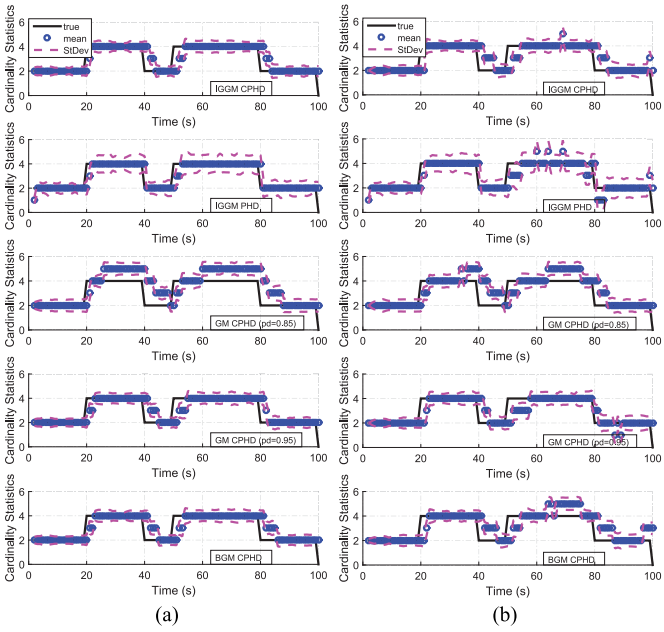

Fig. 7. Average of cardinality estimates in 50 Monte Carlo runs. (a) $\mathrm{SNR}_{th} = 4$. (b) $\mathrm{SNR}_{th} = 5.5$.

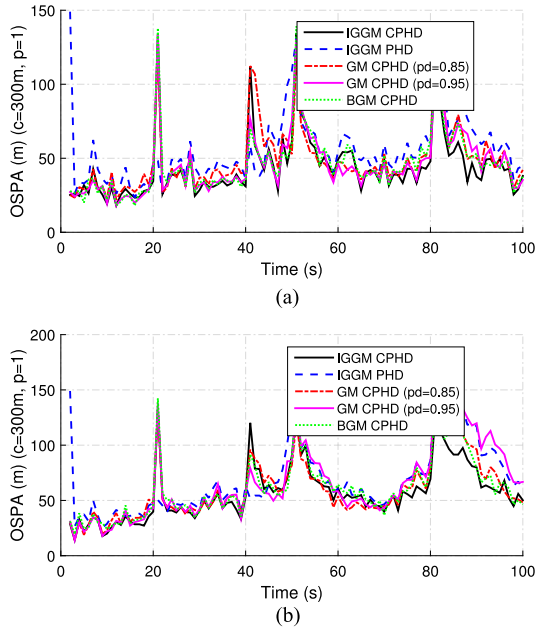

Fig. 8. Average of OSPA distances versus time in 50 Monte Carlo runs. (a) $\mathrm{SNR}_{th} = 4$. (b) $\mathrm{SNR}_{th} = 5.5$.

with $p_{D,k} = 0.95$ and the BGM CPHD filter estimate one more target in $[60, 75]$ s. Fig. 7 also shows us that the standard GM CPHD filters cannot obtain the correct estimates without the correct detection probability. Fig. 8 shows the average OSPA distances versus time of the five filters with different SNR_{th} values. When SNR_{th} is 4, it can be seen that the plots of the IGGM filters are between $[20, 50]$ m in most of the simulation. The IGGM CPHD filter (red curve) and the BGM CPHD filter (green curve) have the same OSPA distance as the GM CPHD filter with appropriate detection probability (pink curve). When SNR_{th} increases to 5.5, the OSPA distances values are higher.

TABLE VII
AVERAGE OF OSPA DISTANCES AND COMPUTATIONAL TIMES

Metrics	OSPA distances		Computational times	
	SNR_{th}		SNR_{th}	
	4	5.5	4	5.5
IGGM CPHD	44.17m	56.94m	17.4s	21.1s
IGGM PHD	54.00m	67.92m	1.6s	1.8s
GM CPHD $p_{D,k} = 0.85$	48.89m	60.52m	17.5s	18.3s
GM CPHD $p_{D,k} = 0.95$	45.95m	65.69m	16.2s	17.3s
BGM CPHD	46.03m	60.56m	18.0s	21.1s

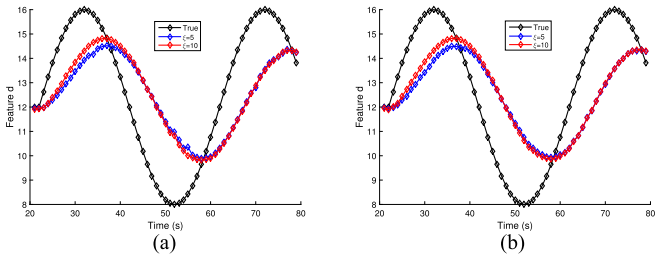

Fig. 9. Average of feature estimates in 50 Monte Carlo runs. (a) $\mathrm{SNR}_{th} = 4$. (b) $\mathrm{SNR}_{th} = 5.5$.

This is primarily because the low detection probability causes more false negatives, increasing the OSPA distances. However, in $[70, 100]$ s, the proposed CPHD filter yields the lowest OSPA values, which means it has the best tracking performance. This conclusion is also validated in Table VII, which shows that the IGGM CPHD filter produces the smallest average OSPA distance indicating the minimum estimation error. The average computational times of the five filters are also shown in Table VII. It can be seen that the four CPHD filters have similar computational costs. This simulation shows that the IGGM CPHD and IGGM PHD filters can produce the correct target cardinality estimates in scenarios where the detection probability is unknown and changing; although the assumption in proposition 2 is not satisfied well, the IGGM CPHD filter can outperform the standard counterpart filter and the BGM CPHD filter, which is the only previous method in the literature to track targets with an unknown detection probability, especially in scenarios where the detection probability is not high enough.

In this simulation, the changing feature d results in dynamically changing $p_{D,k}$. Fig. 9 shows the true feature and the estimates of Target 6. As seen in Fig. 9, the IGGM CPHD filter can accurately estimate the variation in spite of the changing features. The final estimate is determined by the measurement and the prediction value. We could change the parameter in the likelihood function to adjust the degree of dependence to which the measurement influences the final estimate. We can observe that the red curve ($\xi = 10$) is closer to the true value than the blue curve ($\xi = 5$) in Fig. 9. Thus, compared with the standard GM filters, the proposed filters can obtain approximated feature

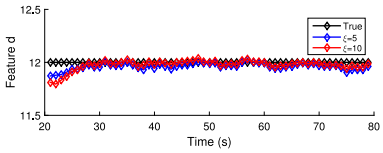

Fig. 10. Average of Gaussian RFS feature estimates in 50 Monte Carlo runs.

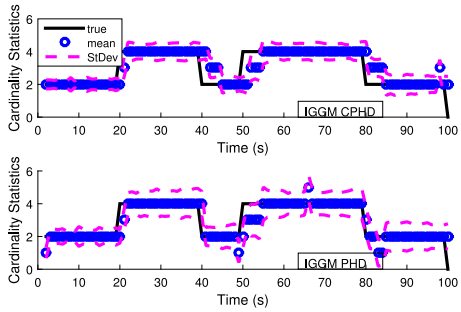

Fig. 11. Average of cardinality estimates with changing clutter parameters.

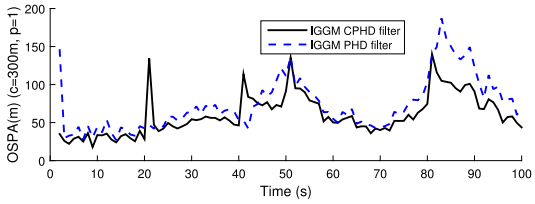

Fig. 12. Average of OSPA distances with changing clutter parameters.

estimates, which will result in more accurate $p_{D,k}$ and better performance than that of the GM CPHD with constant detection probability in the dynamic changing detection probability scenario.

The feature is modeled as a Gaussian RFS whose mean is 12 and variance is 1. The parameter SNR_{th} is 4 in (81). Fig. 10 shows the average of the feature estimates after 50 Monte Carlo runs. It illustrates that the IGGM CPHD filter can yield the correct feature estimates, because the inverse gamma function and the gamma function are approximated as the Gaussian function when the shape parameters have large values.

To validate the robustness of the IGGM filters when the value of the clutter parameter is varying and not accurately known, the ground truth α_k^{κ} and β_k^{κ} are changed to 41 and 280, respectively, while in every frame the filter used parameters modeled as $\alpha_k^{\kappa} \sim \mathcal{N}(\alpha; 31; 9)$ and $\beta_k^{\kappa} \sim \mathcal{N}(\beta; 240; 2500)$. In this changing detection probability scenario, the average results over 50 Monte Carlo runs are shown in Figs. 11 and 12. From the figures, we can observe that the IGGM filters can yield correct cardinality estimates and low location error with some delay in identifying the target cardinality change. This simulation shows the robustness of the IGGM filters to accommodate the mismatched clutter parameters.

2) Nonlinear Bearing and Range Simulation: Here, we study the performance of the two proposed filters in tracking the nonlinear motion of multiple targets with changing and unknown detection probability. Typically, the extended Kalman (EK) filter and unscented Kalman (UK) filter [36]–[38] are the nonlinear approximations to the GM CPHD recursion [4] used

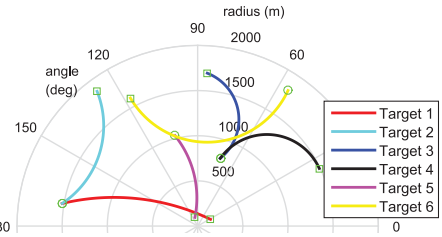

Fig. 13. Trajectories in the $r-\theta$ plane.

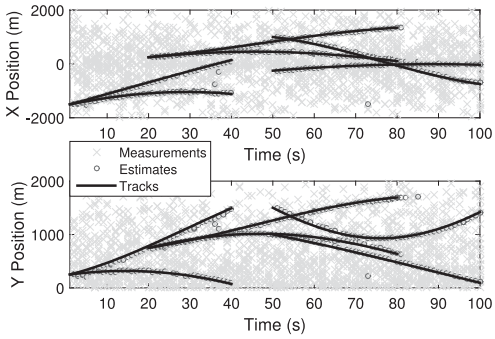

Fig. 14. True tracks, measurements, and filter estimates.

to track nonlinear motion. The multiple-model [39] PHD filter [40] is another commonly-used method. The IGGM CPHD and PHD filters based on unscented transform (UT) are employed in this simulation. The unscented transform IGGM filers can be implemented by propagating the kinematic state and position measurement used in IGGM filters as in the conventional UT CPHD/PHD filters [4].

Consider a six-target scenario whose target tracks are shown in Fig. 13. Each target state consists of kinematic state $\tilde{\mathbf{x}}_k = [p_{x,k}, \dot{p}_{x,k}, p_{y,k}, \dot{p}_{y,k}]^T$, turn rate ω_k, and feature d, i.e., $\mathbf{x}_k = [\tilde{\mathbf{x}}_k, \omega_k, d]^T$. For simplicity, let the union of $\tilde{\mathbf{x}}_k$ and ω_k be $\tilde{\mathbf{x}}_k$, i.e., $\tilde{\mathbf{x}}_k = [\tilde{\mathbf{x}}_k^T, \omega_k]^T$. The sensor measurement is noisy bearing and the range vector $\tilde{\mathbf{z}}_k = [\theta_k, r_k]^T$. The motion model and measurement model of a single target is as described in [4], [9].

The birth process is also a Poisson RFS, and its intensity is (82) with parameters $w_\gamma = 0.03$, $\mathbf{m}_\gamma^{(1)} = [-1500, 0, 250, 0, 0]^T$, $\mathbf{m}_\gamma^{(2)} = [-250, 0, 1000, 0, 0]^T$, $\mathbf{m}_\gamma^{(3)} = [250, 0, 7500, 0, 0]^T$, $\mathbf{m}_\gamma^{(4)} = [1000, 0, 1500, 0, 0]^T$, $P_\gamma = diag([50, 50, 50, 50, 6/180]^T)^2$, $\alpha_\gamma^i = 51$, β_γ^i is 500, 400, 450, and 600 for different values of i. The feature changes following a sine function versus time; the amplitudes are 1.5, 3, 2, 1, 2.5, and 4; and the periods of the sine functions are all $40\delta t$. Suppose that the target $p_{D,k}(d)$ follows (81), and $\mathrm{SNR}_{th} = 4$. The survival probability is $p_{S,k} = 0.99$. Clutter is also modeled as a Poisson RFS. Clutter intensity is expressed as $\kappa_k(\tilde{\mathbf{z}}, h) = \lambda_\kappa c(\tilde{\mathbf{z}}) \mathrm{IG}_k^{\kappa}(d; \alpha_k^{\kappa}; \beta_k^{\kappa}) g_k(h|d)$, where the average clutter intensity $\lambda_\kappa = 3\times10^{-3}(\mathrm{radm})^{-1}$, $c(\tilde{\mathbf{z}}) = Vu(\tilde{\mathbf{z}})$ and $V = 2000\pi$ radm. The parameters in $\mathrm{IG}_k^{\kappa}(d; \alpha_k^{\kappa}; \beta_k^{\kappa})$ are $\alpha_k^{\kappa} = 41$ and $\beta_k^{\kappa} = 280$.

Both UT IGGM CPHD and UT IGGM PHD filters are applied to the same measurement data. Fig. 14 shows the true tracks, the measurements, and the estimates in the X-Y axis. Results of the UT IGGM PHD filter are similar to those of the UT IGGM CPHD filter. The UT IGGM CPHD filter can identify all target births and track the nonlinear motion well without

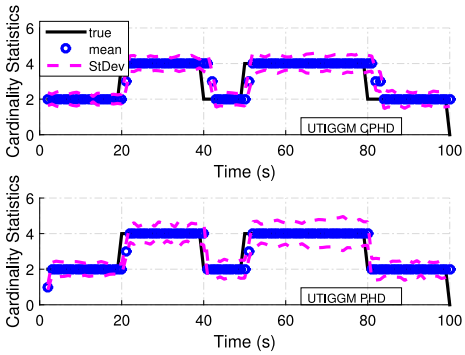

Fig. 15. Average of cardinality estimates in 50 Monte Carlo runs for UT IGGM CPHD and UT IGGM PHD filters.

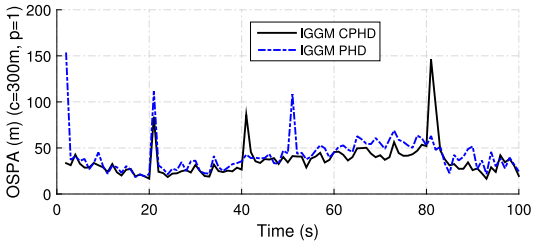

Fig. 16. Average of OSPA distances in 50 Monte Carlo runs for UT IGGM CPHD and UT IGGM PHD filters.

knowing the changing detection probability. In Fig. 15, both filters yield satisfactory target cardinality estimates. In Fig. 16, the low OSPA distances indicate that the proposed filters can obtain good performance in target state estimation.

V. Conclusion

In the standard GM CPHD and GM PHD filters, the target detection probability must be known a priori. In addition, these two standard filters assume that the process noise and measurement noise of the parameters propagated in the recursions are Gaussian distributions. Those limitations may restrict the two filters application in some real problems. To accommodate the unknown target detection probability and nonnegative non-Gaussian parameters, this paper proposed a new closed-form solution to the CPHD and PHD filters based on the inverse gamma Gaussian mixture distribution. We first assumed that the feature parameter (e.g., SNR) is position independent. Then, the nonnegative and non-Gaussian feature parameter, whose posterior probability density and likelihood function are inverse gamma and gamma functions, was incorporated into the recursions to determine detection probability. The merging procedure of the inverse gamma components was also derived to prevent the unbounded increase of mixture components by minimizing the Kullback-Leibler divergence in this paper. The effectiveness of the two IGGM filters was first demonstrated on a real heavy-clutter scenario, which has been used as a benchmark problem for track initialization and target tracking. The experiments showed that the proposed methods with PUB model can confirm the track by frame 32 without known target detection probability and that the same result can be obtained by the standard GM filters with appropriate detection probability, while the standard IMM-MHT and IMM-PDA methods require 38 and 39 frames, respectively. Then, the performances of IGGM CPHD filter and IGGM PHD filter were examined on simulated scenarios. Simulations first showed that the two proposed IGGM filters can converge to the correct number of targets with unknown detection probability and that the proposed filters can achieve the same performance as the standard GM filters that assumes known detection probability in both high and low detection probability scenarios. Second, in the unknown and dynamically changing detection probability scenarios, both IGGM filters can outperform their standard counterpart filters in estimating the number of targets and their kinematic states by introducing the feature. They also outperform the BGM CPHD filter, which was previously proposed to handle unknown detection probability, especially in scenarios where the detection probability is low. The robustness of the proposed filters was validated by real data and simulation scenarios. It was also shown that the analytical and empirical computational complexities of the proposed filters have the same order as those of their standard counterparts.

Appendix A
Proof of Proposition 2

First, let us prove the below equation:

$$\int_0^\infty p_{D,k}(x)\mathrm{IG}(x;\alpha;\beta)dx \approx p_{D,k}\left(\int_0^\infty x\mathrm{IG}(x;\alpha;\beta)dx\right). \tag{A.1}$$

When $p_{D,k}(\cdot)$ is relatively constant around the mean of the IG function or $\mathrm{IG}(x;\alpha;\beta)$ is approximating to Dirac delta function, the right-hand side of A.1 will be a good approximation for the left-hand side. So we assume that the $p_{D,k}$ do not change rapidly. Additionally, if the shape parameter of IG distribution has a large value, the variance will be small. This will result in the IG distribution being much closer to Dirac delta function. Based on A.1,

$$\begin{aligned}&\left\langle p_{D,k}, w_{k|k-1}\mathcal{N}(\cdot;\mathbf{m};P)\mathrm{IG}(\cdot;\alpha;\beta)\right\rangle\\ &= w_{k|k-1}\int_0^\infty p_{D,k}(y)\mathrm{IG}(y;\alpha;\beta)dy\int_{-\infty}^\infty \mathcal{N}(\tilde{\mathbf{x}};\mathbf{m};P)d\tilde{\mathbf{x}}\\ &\approx w_{k|k-1}p_{D,k}(d_{k|k-1})\end{aligned} \tag{A.2}$$

where $d_{k|k-1}$ is the mean of IG distribution.

Equation (47) can be obtained by substituting (44) into (9). Also, the $\langle v,\psi_{k,\mathbf{z}}\rangle$ in (10) can be simplified as

$$\begin{aligned}&\langle v,\psi_{k,\mathbf{z}}\rangle\\ &= \int\sum_{i=1}^{J_{k|k-1}} w_{k|k-1}^{(i)}\mathcal{N}(\tilde{\mathbf{x}};\mathbf{m}_{k|k-1}^{(i)};P_{k|k-1}^{(i)})\\ &\cdot \mathrm{IG}(y;\alpha_{k|k-1}^{(i)};\beta_{k|k-1}^{(i)})\frac{\langle 1,\kappa_k\rangle}{\kappa_k(\mathbf{z})}g_k(\mathbf{z}|\mathbf{x})p_{D,k}(\mathbf{x})d\mathbf{x}\\ &= \sum_{i=0}^{J_{k|k-1}} w_{k|k-1}^{(i)}\frac{\langle 1,\kappa_k\rangle}{\kappa_k(\tilde{\mathbf{z}},h)}\int_0^\infty p_{D,k}(y)\mathrm{IG}(y;\alpha_{k|k-1}^{(i)};\beta_{k|k-1}^{(i)})\\ &\cdot g_k(h|y)dy\int_{-\infty}^\infty \mathcal{N}(\tilde{\mathbf{x}};\mathbf{m}_{k|k-1}^{(i)};P_{k|k-1}^{(i)})\tilde{g}_k(\tilde{\mathbf{z}}|\tilde{\mathbf{x}})d\tilde{\mathbf{x}}\end{aligned} \tag{A.3}$$

where $g_k(\cdot)$ and $\tilde{g}_k(\cdot)$ are measurement likelihoods corresponding to feature and kinematic state, respectively. Based on (31) and (32),

$$\langle v, \psi_{k,\mathbf{z}} \rangle = \sum_{i=1}^{J_{k|k-1}} w_{k|k-1}^{(i)} \frac{\langle 1, \kappa_k \rangle}{\kappa_k(\tilde{\mathbf{z}}, h)} q_k^{(i)}(\tilde{\mathbf{z}}) \chi_{v,k}^{(i)}(h) p_{D,k}(d_{k|k-1}^{(i)}), \tag{A.4}$$

and $\kappa_k(\tilde{\mathbf{z}}, h)$ is given by (30) denoting the intensity of clutter measurements at time k. Also, $\psi_{k,\mathbf{z}}^{(j)} = \psi_{k,[\tilde{\mathbf{z}},h]^T}^{(j)} = \frac{\langle 1,\kappa_k \rangle}{\kappa_k(\tilde{\mathbf{z}},h)} q_k^{(i)}(\tilde{\mathbf{z}})$ $\chi_{v,k}^{(i)}(h) p_{D,k}(d_{k|k-1}^{(i)})$. Substituting $\psi_{k,\mathbf{z}}^{(j)}$ and $v_{k|k-1}(\mathbf{x}) q_{D,k}(\mathbf{x})$ into (7), (58) and (59) can be obtained.

Appendix B
Proof of Equation (70)

If given an inverse gamma distribution function $\mathrm{IG}(x; \alpha; \beta)$, then, the expected value of $\log x$ is

$$E[\log x] = \log \beta - \varphi_0(\alpha) \tag{B.1}$$

where $\varphi_0(\cdot)$ is the digamma function or the 0-order polygamma function. The expected value of $1/x$ is

$$E\left[1/x\right] = \alpha/\beta \tag{B.2}$$

Proof: The moment generating function of y is defined as

$$\mu_y(s) = E[e^{sy}] \tag{B.3}$$

where y is a univariate random variable. Let $y = \log x$, and x be an inverse gamma distribution function with parameters α, β i.e., $x \sim \mathrm{IG}(x; \alpha; \beta)$. Then, the moment generating function of y is

$$\begin{aligned}\mu_y(s) = E[x^s] &= \int x^s \frac{\beta^\alpha}{\Gamma(\alpha)} x^{-\alpha-1} \exp\left(-\frac{\beta}{x}\right) dx \\ &= \frac{\beta^\alpha}{\Gamma(\alpha)} \frac{\Gamma(\alpha - s)}{\beta^{\alpha-s}} \int \frac{\beta^{\alpha-s}}{\Gamma(\alpha-s)} x^{-(\alpha-s)-1} \exp\left(-\frac{\beta}{x}\right) dx \\ &= \frac{\beta^\alpha}{\Gamma(\alpha)} \frac{\Gamma(\alpha-s)}{\beta^{\alpha-s}} = \frac{\Gamma(\alpha-s)}{\Gamma(\alpha)} \beta^s. \end{aligned} \tag{B.4}$$

The expected value of y is

$$E[y] = \frac{d\mu_y(s)}{ds}|_{s=0}. \tag{B.5}$$

Hence, we can obtain the expected value of $\log x$ as

$$\begin{aligned} E[y] = E[\log x] &= \frac{d}{ds}\left(\frac{\Gamma(\alpha-s)}{\Gamma(\alpha)} \beta^s\right)|_{s=0} \\ &= \log\beta - \varphi_0(\alpha). \end{aligned} \tag{B.6}$$

Substituting $y = 1/x$ into (B.3), we can obtain the moment generating function of $1/x$.

$$\begin{aligned}\mu_y(s) = E[e^{s/x}] &= \int \frac{\beta^\alpha}{\Gamma(\alpha)} x^{-\alpha-1} \exp\left(-\frac{\beta}{x}\right) \exp\left(\frac{s}{x}\right) dx \\ &= \frac{\beta^\alpha}{(\beta-s)^\alpha} \int \frac{(\beta-s)^\alpha}{\Gamma(\alpha)} x^{-\alpha-1} \exp\left(-\frac{\beta-s}{x}\right) dx \\ &= \frac{\beta^\alpha}{(\beta-s)^\alpha}. \end{aligned} \tag{B.7}$$

Then, we can obtain the expected value of $1/x$

$$E\left[1/x\right] = \frac{d}{ds}\left(\frac{\beta^\alpha}{(\beta-s)^\alpha}\right)|_{s=0} = \frac{\alpha}{\beta}. \tag{B.8}$$

References

[1] R. Mahler, "Multi-target Bayes filter via first-order multi-target moments," *IEEE Trans. Aerosp. Electron. Syst.*, vol. 39, no. 4, pp. 1152–1178, Oct. 2003.

[2] R. Mahler, "PHD filters of higher order in target number," *IEEE Trans. Aerosp. Electron. Syst.*, vol. 43, no. 4, pp. 1523–1543, Oct. 2007.

[3] R. Mahler, *Statistical Multisource Multitarget Information Fusion.* Norwood, MA, USA: Artech House, 2007.

[4] B.-T. Vo, B.-N. Vo, and A. Cantoni, "Analytic implementations of the cardinalized probability hypothesis density filter," *IEEE Trans. Signal Process.*, vol. 55, no. 7, pp. 3553–3567, Jul. 2007.

[5] B.-N. Vo and W.-K. Ma, "The Gaussian mixture probability hypothesis density filter," *IEEE Trans. Signal Process.*, vol. 54, no. 11, pp. 4091–4104, Nov. 2006.

[6] B.-N. Vo, S. Singh, and A. Doucet, "Sequential Monte Carlo methods for multi-target filtering with random finite sets," *IEEE Trans. Aerosp. Electron. Syst.*, vol. 41, no. 4, pp. 1224–1245, Oct. 2005.

[7] R. Mahler, "CPHD and PHD filters for unknown backgrounds, II: Multi-target filtering in dynamic clutter," *Proc. SPIE*, vol. 7330, 2009, Art. no. 73300L.

[8] R. Mahler and A. El-Fallah, "CPHD and PHD filters for unknown backgrounds, III: Tractable multitarget filtering in dynamic clutter," *Proc. SPIE*, vol. 7698, 2010, Art. no. 76980F.

[9] R. Mahler, B.-T. Vo, and B.-N. Vo, "CPHD filtering with unknown clutter rate and detection profile," *IEEE Trans. Signal Process.*, vol. 59, no. 8, pp. 3497–3513, Aug. 2011.

[10] X. Chen, R. Tharmarasa, M. Pelletier, and T. Kirubarajan, "Integrated clutter estimation and target tracking using Poisson point processes," *IEEE Trans. Aerosp. Electron. Syst.*, vol. 48, no. 2, pp. 1210–1235, Apr. 2012.

[11] R. Mahler and B.-T. Vo, "An improved CPHD filter for unknown clutter backgrounds," *Proc. SPIE*, vol. 9091, 2014, Art. no. 90910B.

[12] R. Mahler, "CPHD filters for unknown clutter and target-birth processes," *Proc. SPIE*, vol. 9091, 2014, Art. no. 90910C.

[13] B. Ristic, D. Clark, and B.-N. Vo, "Improved SMC implementation of the PHD filter," in *Proc. Int. Conf. Inf. Fusion*, Edinburgh, U.K., Jul. 2010, pp. 1–8.

[14] B. Ristic, D. Clark, and B.-N. Vo, "Adaptive target birth intensity in PHD and CPHD filters," *IEEE Trans. Aerosp. Electron. Syst.*, vol. 48, no. 2, pp. 1656–1668, Apr. 2012.

[15] J. Houssineau and D. Laneuville, "PHD filter with diffuse spatial prior on the birth process with applications to GM-PHD filter," in *Proc. Int. Conf. Inf. Fusion*, Edinburgh, U.K., Jul. 2010, pp. 1–8.

[16] M. Beard, B.-T. Vo, B.-N. Vo, and S. Arulampalam, "Gaussian mixture PHD and CPHD filtering with partially uniform target birth," in *Proc. Int. Conf. Inf. Fusion*, Singapore, Jul. 2012, pp. 535–541.

[17] M. Beard, B.-T. Vo, B.-N. Vo, and S. Arulampalam, "A partially uniform target birth model for Gaussian mixture PHD/CPHD filtering," *IEEE Trans. Aerosp. Electron. Syst.*, vol. 49, no. 4, pp. 2835–2844, Oct. 2013.

[18] G. Papa, P. Braca, S. Horn, S. Marano, V. Matta, and P. Willett, "Multisensor adaptive Bayesian tracking under time-varying target detection probability," *IEEE Trans. Aerosp. Electron. Syst.*, vol. 52, no. 5, pp. 2193–2209, Oct. 2016.

[19] F. Meyer, P. Braca, F. Hlawatsch, M. Micheli, and K. LePage, "Scalable adaptive multitarget tracking using multiple sensors," in *Proc. IEEE GLOBECOM*, Washington, D.C., USA, Dec. 2016, pp. 1–6.

[20] B.-T. Vo, B.-N. Vo, R. Hoseinnezhad, and R. Mahler, "Robust multi-Bernoulli filtering," *IEEE J. Sel. Topics Signal Process.*, vol. 7, no. 3, pp. 399–409, Jun. 2013.

[21] D. Lerro and Y. Bar-Shalom, "Automated tracking with target amplitude information," in *Proc. Amer. Control Conf.*, San Diego, CA, USA, 1990, pp. 2875–2880.

[22] G. van Keuk, "Multihypothesis tracking using incoherent signal strength information," *IEEE Trans. Aerosp. Electron. Syst.*, vol. 32, no. 3, pp. 1164–1170, Jul. 1996.

[23] D. Clark, B. Ristic, B.-N. Vo, and B.-T. Vo, "Bayesian multi-object filtering with amplitude feature likelihood for unknown object SNR," *IEEE Trans. Signal Process.*, vol. 58, no. 1, pp. 26–37, Jan. 2010.

[24] V. Kılıç, M. Barnard, W. Wang, A. Hilton, and J. Kittler, "Mean-shift and sparse sampling-based SMC-PHD filtering for audio informed visual speaker tracking," *IEEE Trans. Multimedia*, vol. 18, no. 12, pp. 2417–1431, Dec. 2016.
[25] P. Borwein and T. Erdélyi, *Polynomials and Polynomial Inequalities*. New York, NY, USA: Springer-Verlag, 1995.
[26] K. Granström and U. Orguner, "Estimation and maintenance of measurement rates for multiple extended target tracking," in *Proc. Int. Conf. Inf. Fusion*, Singapore, Jul. 2012, pp. 2170–2176.
[27] A. R. Runnalls, "Kullback-Leibler approach to Gaussian mixture reduction," *IEEE Trans. Aerosp. Electron. Syst.*, vol. 43, no. 3, pp. 989–999, Jul. 2007.
[28] D. Schieferdecker and M. F. Huber, "Gaussian mixture reduction via clustering," in *Proc. Int. Conf. Inf. Fusion*, Seattle, WA, USA, Jul. 2009, pp. 1536–1543.
[29] J. Stoer and R. Bulirsch, *Introduction to Numerical Analysis*, 2nd ed. New York, NY, USA: Springer-Verlag, 1993.
[30] S. H. Roszkowski, "Common database for tracker comparison," in *Signal Data Process. Small Targets 1998, SPIE Proc.*, vol. 3373, 1998, doi: 10.1117/12.324610.
[31] J. Cai, A. Sinha, and T. Kirubarajan, "EM-ML algorithm for track initialization using possibly noninformative data," *IEEE Trans. Aerosp. Electron. Syst.*, vol. 41, no. 3, pp. 1030–1048, Jul. 2005.
[32] M. R. Chummun, Y. Bar-Shalom, and T. Kirubarajan, "Adaptive early-detection ML-PDA estimator for LO targets with EO sensors," *IEEE Trans. Aerosp. Electron. Syst.*, vol. 38, no. 2, pp. 694–707, Apr. 2002.
[33] R. Popoli and S. S Blackman, *Design and Analysis of Modern Tracking Systems*. Dedham, MA, USA: Artech House, 1999.
[34] D. Lerro and Y. Bar-Shalom, "IR target detection and clutter reduction using the interacting multiple model estimator," *Proc. SPIE*, vol. 3373, pp. 216–221, 1988.
[35] D. Schuhmacher, B.-T. Vo, and B.-N. Vo, "A consistent metric for performance evaluation of multi-object filters," *IEEE Trans. Signal Process.*, vol. 56, no. 8, pp. 3447–3457, Aug. 2008.
[36] A. H. Jazwinski, *Stochastic Processes and Filtering Theory*. New York, NY, USA: Academic, 1970.
[37] B. D. Anderson and J. B. Moore, *Optimal Filtering*. Englewood Cliffs, NJ, USA: Prentice-Hall, 1979.
[38] S. J. Julier and J. K. Uhlmann, "Unscented filtering and nonlinear estimation," *Proc. IEEE*, vol. 92, no. 3, pp. 401–422, Mar. 2004.
[39] G. A. Ackerson and K. S. Fu, "On state estimation in switching environments," *IEEE Trans. Autom. Control*, vol. AC-15, no. 1, pp. 10–17, Feb. 1970.
[40] K. Punithakumar, T. Kirubarajan, and A. Sinha, "Multiple-model probability hypothesis density filter for tracking maneuvering targets," *IEEE Trans. Aerosp. Electron. Syst.*, vol. 44, no. 1, pp. 87–98, Jan. 2008.

Chenming Li received the B.S. degree from the Beihang University (BUAA), Beijing, China, in 2012. He is currently working toward the Ph.D degree at the School of Electronic and Information Engineering, BUAA. His research interests include target detection and tracking, and image processing.

Wenguang Wang received the B.S. degree from Jianghan Petrolum University, Jingzhou, China, in 1997, and the Ph.D. degree from Beihang University, Beijing, China, in 2007. He is currently an Associate Professor with the School of Electronic and Information Engineering, Beihang University. His research interests include signal processing, target detection and tacking, image understanding, and so on.

Thia Kirubarajan (S'95–M'98–SM'03) was born in Sri Lanka in 1969. He received the B.A. and M.A. degrees in electrical and information engineering from Cambridge University, Cambridge, U.K., in 1991 and 1993, and the M.S. and Ph.D. degrees in electrical engineering from the University of Connecticut, Storrs, CT, USA, in 1995 and 1998, respectively. He is currently a Professor in the Department of Electrical and Computer Engineering, McMaster University, Hamilton, ON, Canada. His research interests include estimation, target tracking, multisource information fusion, sensor resource management, signal detection, and fault diagnosis. His research activities are supported by U.S. Missile Defense Agency, U.S. Office of Naval Research, NASA, Qualtech Systems, Inc., Raytheon Canada, Ltd., and Defense Research Development Canada, Ottawa. In September 2001, he served in a DARPA expert panel on unattended surveillance, homeland defense, and counterterrorism. He has also served as a Consultant in these areas to a number of companies, including Motorola Corporation, Northrop-Grumman Corporation, Pacific-Sierra Research Corporation, Lockhead Martin Corporation, Qualtech Systems, Inc., Orincon Corporation, and BAE systems. He has worked on the development of a number of engineering software programs, including BEARDAT for target localization from bearing and frequency measurements in clutter and FUSEDAT for fusion of multisensor data for tracking. He has also worked with Qualtech Systems, Inc., to develop an advanced fault diagnosis engine. Dr. Kirubarajan has published more than 360 articles in the areas of his research interests, in addition to one book on estimation, tracking and navigation, four edited volumes, and 12 book chapters. He received IEEE Barry Award and Ontario Premiers Research Excellence Award. Since 2004, he is a Canada Research Chair in Information Fusion.

Jinping Sun received the M.Sc. and Ph.D. degrees from the Beihang University (BUAA), Beijing, China, in 1998 and 2001, respectively. He is currently a Professor with the School of Electronic and Information Engineering, BUAA. His research interests include high-resolution radar signal processing, target tracking, image understanding, and robust beamforming.

Peng Lei received the B.S. and Ph.D. degrees in electrical engineering from Beihang University, Beijing, China, in 2006 and 2012, respectively. He is currently an Assistant Professor with the School of Electronic and Information Engineering, Beihang University. His research interests include signal processing, especially in time-frequency analysis and spectral estimation, image processing, and target recognition. He was the recipient of the 2011 IEEE IGARSS Student Travel Grant.